HHS Public Access

Author manuscript

Cell Rep. Author manuscript; available in PMC 2022 April 13.

Published in final edited form as:

Cell Rep. 2022 March 29; 38(13): 110560. doi:10.1016/j.celrep.2022.110560.

Neutral ceramidase-dependent regulation of macrophage metabolism directs intestinal immune homeostasis and controls enteric infection

Rui Sun[1,2,3], **Xuemei Gu**[3], **Chao Lei**[1,3], **Liang Chen**[1,3], **Shenghui Chu**[4], **Guangzhong Xu**[4], **Mark A. Doll**[5], **Yi Tan**[6], **Wenke Feng**[4,5,7,8], **Leah Siskind**[3,5], **Craig J. McClain**[4,5,7,8,9], **Zhongbin Deng**[1,3,7,8,10,*]

[1]Department of Surgery, Division of Immunotherapy, University of Louisville, CTRB 311, 505 South Hancock Street, KY 40202, USA

[2]Department of Oncology, Wuhan Fourth Hospital, Puai Hospital, Tongji Medical College, Huazhong University of Science and Technology, Wuhan 430033, China

[3]Brown Cancer Center, University of Louisville, Louisville, KY 40202, USA

[4]Department of Medicine, University of Louisville, Louisville, KY 40202, USA

[5]Department of Pharmacology & Toxicology, University of Louisville, Louisville, KY 40202, USA

[6]Department of Pediatrics, University of Louisville, Louisville, KY 40202, USA

[7]Alcohol Research Center, University of Louisville, Louisville, KY 40202, USA

[8]Hepatobiology & Toxicology Center, University of Louisville, Louisville, KY 40202, USA

[9]Robley Rex VA Medical Center, Louisville, KY, USA

[10]Lead contact

SUMMARY

It is not clear how the complex interactions between diet and intestinal immune cells protect the gut from infection. Neutral ceramidase (NcDase) plays a critical role in digesting dietary sphingolipids. We find that NcDase is an essential factor that controls intestinal immune cell dynamics. Mice lacking NcDase have reduced cluster of differentiation (CD) $8\alpha\beta^+$ T cells and interferon (IFN)-γ^+ T cells and increased macrophages in the intestine and fail to clear bacteria after *Citrobacter rodentium* infection. Mechanistically, cellular NcDase or extracellular vesicle (EV)-related NcDase generates sphingosine, which promotes macrophage-driven Th1 immunity. Loss of NcDase influences sphingosine-controlled glycolytic metabolism in macrophages,

*Correspondence: zhongbin.deng@louisville.edu.

AUTHOR CONTRIBUTIONS

R.S. and Z.D. designed the study, analyzed and interpreted the data, and prepared the manuscript; R.S., X.G., L.C., S.C., and G.X. performed the experiments and interpreted the data; C.L. provided technical support for bacterial culture; M.D. provided technical support; Y.T., W.F., L.S., and C.M. interpreted the findings.

SUPPLEMENTAL INFORMATION

Supplemental information can be found online at https://doi.org/10.1016/j.celrep.2022.110560.

DECLARATION OF INTERESTS

The authors declare no competing interests.

which regulates the bactericidal activity of macrophages. Importantly, administration of dietary sphingomyelin and genetic deletion or pharmacological inhibition of SphK1 can protect against *C. rodentium* infection. Our findings demonstrate that sphingosine profoundly alters macrophage glycolytic metabolism, leading to intestinal macrophage activation and T cell polarization, which prevent pathogen colonization of the gut.

In brief

Sun et al. find that neutral ceramidase sculpts the intestinal immune landscape and drives macrophage metabolic function and, consequently, glycolysis-dependent PP2A-controlled inflammasome activation, IL-1β production, and bactericidal activity of macrophages. These data describe an intestine-intrinsic interplay between sphingolipid metabolites and gut nutritional immunity against a mucosal pathogen.

Graphical Abstract

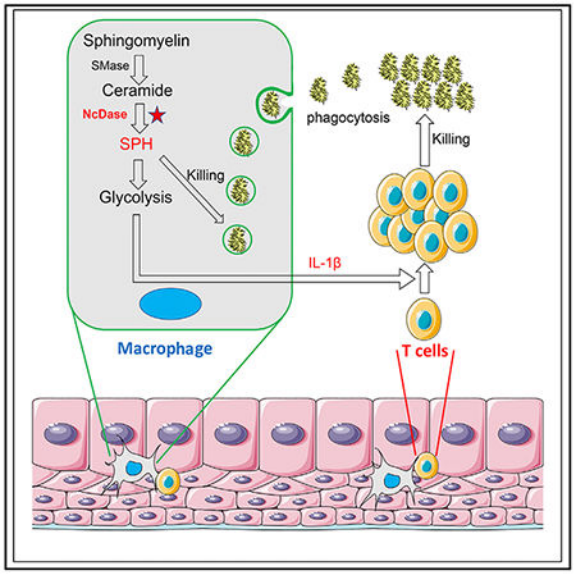

INTRODUCTION

Enteric infections commonly associate with intestinal epithelial cells (IECs), intestinal immune components, and food (Pham and Lawley, 2014; Ramanan and Cadwell, 2016). The enteric infections have been ascribed to dysfunction of host immune systems and community of gut microbes, which are unable to effectively prevent pathogen colonization (Kim et al., 2017). Therefore, deciphering the innate mechanisms that drive local immunity and host defense against enteric pathogens is critical for developing approaches for treating and preventing infection.

Diet, including dietary sphingolipid (Duan and Nilsson, 2009), is the important regulator of the gut microenvironment. A major challenge in understanding the immunological consequences of diet is that the complexity of diets makes it difficult to determine molecular mechanisms. Sphingolipids are a family of metabolic lipids that are essential structural

components of intestinal membranes, providing protection and integrity to the intestinal mucosa and regulating intestinal absorption processes (Maceyka and Spiegel, 2014). Studies using common acute and chronic epithelial injury colitis models have shown that bioactive sphingolipids, particularly sphingomyelin (SM), ceramide, and sphingosine-1-phosphate (S1p), are important regulators of inflammation in inflammatory bowel disease (IBD) (Liang et al., 2013). The brush border enzyme, neutral ceramidase (NcDase), catalyzes the hydrolysis of ceramide, the central molecule in the sphingolipid metabolism, to sphingosine (Kono et al., 2006). Despite the interaction of dietary sphingolipids with IECs and gut microbiota, little is known about the mechanisms regulating how NcDase and its metabolite sphingosine instructs or manipulates local protective immune responses to enteric pathogens.

Citrobacter rodentium is a relative of enteropathogenic *Escherichia* coli (EPEC), a food- and water-borne non-invasive enteric pathogen that infects the murine large intestine with a pathology associated with IBD in humans (Collins et al., 2014) (Koroleva et al., 2015). Susceptibility to *C. rodentium* infection is critically dependent on host innate immune responses and the T-helper (Th) 1 inflammatory response (Navabi et al., 2017; Schreiber et al., 2013). Interferon-γ (IFN-γ), the prototypic Th1 cell effector cytokine, is crucial for clearance of intracellular pathogens and also can induce tissue pathology associated with infectious disease (Dolowschiak et al., 2016). However, how sphingosine tightly regulates IFN-γ to mediate pathogen clearance while limiting unintended tissue damage remains poorly understood.

Macrophages exhibit metabolic and functional plasticity (Van den Bossche et al., 2017). While aerobic glycolysis is a defining characteristic of “inflammatory” M1 macrophages (Langston et al., 2019), “alternative” M2 macrophages rely on mitochondrial fatty-acid oxidation (FAO) to fuel oxidative phosphorylation (Huang et al., 2014). Emerging evidence indicates that glycolysis is involved in NLRP3 inflammasome activation in macrophages (Moon et al., 2015; Xie et al., 2016). Inflammasome plays a critical role in the activation of caspase-1 in response to a variety of agonists, including sphingosine (Luheshi et al., 2012) and bacterial toxins (Tschopp and Schroder, 2010)’. However, the molecular mechanisms linking sphingosine with macrophage metabolism and phagocytosis to the inflammasome activation are not being investigated. Using a colitis-associated colon cancer model and alcohol-/non-alcohol-induced gut inflammation experiments, we have recently shown that NcDase and metabolites sphingosine/S1p play a critical role in the regulation of gut Th17 cells and B cells (Chu et al., 2021; Gu et al., 2021).

In this study, we showed NcDase dynamically coordinates immune cells in the intestine and confers dramatic protection from mucosal bacterial infections. We demonstrated that sphingosine has direct antimicrobial activity and immunomodulatory activities on macrophages that in turn drive mucosal IFN-γ^+ T cell responses. We determined NcDase or its metabolite sphingosine-induced glycolysis acts as an essential metabolic mechanism for PP2A-dependent inflammasome activation and the maturation and secretion of interleukin (IL)-1β. Administration of dietary sphingomyelin prevents *C. rodentium*-induced colitis.

RESULTS

NcDase expression shapes the intestinal immune landscape

To explore the role of NcDase in intestinal immune homeostasis, we characterized the immune cell composition of NcDase-deficient mice using cytometry by time of flight (CyTOF) and flow cytometry analysis of lamina propria lymphocytes (LPLs) in the small intestine (SI) and large intestine (LI). The majority of cell clusters includes $CD8^+$ T cells, $CD4^+$ T cells, macrophages, monocytes, B cells, or dendritic cells (DCs) (Figure 1A). We observed a substantial decrease in $CD8^+$ T cells (cluster 7). In contrast, $CD11b^+CD11c^{low}MHCII^-F4/80^{hi}$ macrophages (cluster 3), $B220^+$ B cells (cluster 4), and $CD4^+$ T cells (cluster 5) were increased in the LPLs (Figures 1B, S1A, and S1B). $CD8^+$ T cells in the intestine include conventional $CD8\alpha\beta^+$ T cells and unconventional $CD8\alpha\alpha^+$ T cells. Fluorescence-activated cell sorting (FACS) analysis showed that the percentage and the absolute number of conventional $CD8\alpha\beta^+$ T cells in the LPLs of $NcDas^{-/-}$ mice were significantly reduced relative to wild-type (WT) mice (Figures 1C and 1D). We further analyzed the populations in the intraepithelial lymphocytes (IELs). $NcDase^{-/-}$ mice also had a significant reduction in the proportion and the total number of $CD8\alpha\beta^+$ T cells in the IEL (Figures S1C and S1D). However, the number and proportion of unconventional $CD8\alpha\alpha^+$ T cells, including both $TCR\alpha\beta^+$ and $TCR\gamma\delta^+$ T cells, were not significantly altered in the IEL (Figures S1C–S1E). We next compared intestinal $CD8\alpha\beta^+$ T, $CD4^+$ T cell subset composition in $NcDas^{-/-}$ and WT mice. Strikingly, IFN-γ^+ IL-$17A^-$ $CD4^+$ T (Th1) cells (Figures 1E and 1F) and IFN-$\gamma^+CD8\alpha\beta^+$ T cells (Figures S2A and S2B) were reduced significantly in the SI-LPL and LI-LPL of $NcDas^{-/-}$ mice, while the similar proportions of $Foxp3^+CD4^+$ T cells and increased number of Th17 cells were found in LI-LPLs of $NcDase^{-/-}$ mice (Figures 1F and S2C). Granzyme B expression, which can directly induce the death of intracellular bacteria, was also reduced in $TCR\alpha\beta^+$ and $TCR\gamma\delta^+$ T cells in the SI-IEL of $NcDase^{-/-}$ mice (Figures S2A and S2B).

We further determined whether the reduction in conventional $CD8\alpha\beta^+$ or IFN-γ^+ T cells in the intestine of $NcDase^{-/-}$ mice was a result of T cell extrinsic or intrinsic effects by mixed bone marrow (BM) chimeras, namely transferring a 1:1 ratio of BM from WT ($CD45.1^+$) and $NcDase^{-/-}$ ($CD45.2^+$) mice into WT recipients ($CD45.1^+CD45.2^+$). Recipient mice with WT BM transferred to WT mice (*WT* → *WT*) and mice with NcDas−/− BM to $NcDase^{-/-}$ mice (*KO* → *KO*) were set as controls. Eight weeks after reconstitution, $CD8\alpha\beta^+$ IEL and LPLs derived from $NcDas^{-/-}$ (45.2) BM were readily detected in the SI and LI of the mixed BM chimeras and have higher levels compared with those from *KO* → *KO* mice (Figures 1G and S2D), but have similar levels compared with those derived from WT (45.1) BM or *WT* → *WT* mice (Figures 1G and S2D). IFN-γ-producing $CD4^+$ T cells (Figures 1H and S2E) and $CD8\alpha\beta^+$ T cells (not shown) were also significantly higher in the SI-LPLs and LI-LPLs of from $NcDase^{-/-}$ BM (45.2) in mixed BM chimeras compared with that of *KO* → *KO* mice. Furthermore, naive splenic $CD4^+$ T cells from $NcDase^{-/-}$ and WT mice differentiated equally well into IFN-γ-producing Th1 cells *in vitro* (Figure S2F). Thus, the paucity of $CD8\alpha\beta^+$ IELs and LPLs and the induction of IFN-γ^+ T cells in $NcDase^{-/-}$ mice were primarily due to T cell extrinsic effects. Taken together, these results indicate that

NcDase or its metabolite exerts effects on innate and adaptive immunity in the intestine where neutral ceramidase is most abundant.

NcDase protects against *C. rodentium* infection by regulating mucosal immunity response

In contrast to IL-22, which provides protection against early *C. rodentium* colonization, IFN-γ in collaboration with IL-21 plays a critical role in protection against *C. rodentium* both early and late in the infection (Solaymani-Mohammadi and Berzofsky, 2019). We next examined the responses of NcDase$^{-/-}$ mice and their WT littermates to oral infection with *C. rodentium*. NcDase$^{-/-}$ mice infected with *C. rodentium* showed a significantly increased burden of fecal bacteria and enhanced production of fecal lipocalin-2 for intestinal inflammation compared with WT mice (Figures 2A and 2B). Indeed, NcDase$^{-/-}$ mice exhibited more severe colonic pathology associated with *C. rodentium* infection, characterized by higher histologic scores, exaggerated submucosal edema, leukocyte expansion of the lamina propria, and mucosal hyperplasia (Figure 2C). NcDase$^{-/-}$ mice were also not able to control bacterial dissemination to peripheral organs (Figure 2D). Importantly, multifocal hepatocellular necrosis with embolic microabscessation were observed in some livers of NcDase$^{-/-}$ mice, while none were seen in the livers of WT mice (Figure 2E).

Consistent with phenotypes in the steady state, NcDase$^{-/-}$ mice exhibited defective induction of IFN-γ in the gut (Figure 2F). The IL-22 response was unaffected and Th17 cells were slightly increased after infection (Figures S3A and S3B), whereas Th1 cells were significantly impaired in the colonic LPL of NcDase$^{-/-}$ mice (Figure S3B). Moreover, IFN-γ-producing CD8γ^{+} LPLs and γδ T cell receptor (TCR) β^{+} IELs were also reduced within the ileum of NcDase$^{-/-}$ mice (Figures S3C and S3D). Collectively, these data demonstrate that expression of NcDase is required for local IFN-γ-producing LPLs during an enteric infection. To test whether impaired IFN-γ induction in the colon may contribute to increased susceptibility of NcDase$^{-/-}$ mice to *C. rodentium* infection, a Th1-inducing immunostimulatory oligonucleotide (ISS-ODN), ODN-BW006, was administered intraperitoneally on days 3 and 5 post infection. ODN BW006 is a synthetic oligonucleotide that contains unmethylated CpG dinucleotides, in particular sequence contexts (CpG motifs), that are recognized by TLR9, leading to strong immunostimulatory effects via induction of IFN-γ (Ciorba et al., 2010; Navabi et al., 2017). ISS-ODN partially restored IFN-γ levels in the colons of *C. rodentium*-infected NcDase$^{-/-}$ mice (Figure 2G). Further, ISS-ODN treatment of NcDase$^{-/-}$ mice constitutively resulted in improved regulation of *C. rodentium* infection (Figure 2H).

IFN-γ^{+} T cells have been associated with the degree of colonization resistance and severity of gastrointestinal disease during *Salmonella typhimurium* infection (Dolowschiak et al., 2016; Thiemann et al., 2017). We further investigated whether NcDase-mediated IFN-γ immune response is required for host defense against *S. typhimurium*. Age- and gender-matched WT littermate or NcDase$^{-/-}$ mice were pretreated with a single dose of streptomycin and orally infected 24 h later with *S. typhimurium*. NcDase$^{-/-}$ mice showed the highest weight reduction (Figure S3E) and lowest survival rate (Figure S3F). NcDase$^{-/-}$ mice also had greater loads of *Salmonella* bacteria in the liver and cecum than did WT

mice after infection (Figure S3G). We further found that NcDase$^{-/-}$ mice exhibited defective induction of CD4^{+}IFN-γ^{+} and CD8αβ^{+}IFN-γ^{+} T cells in the colon (Figure S3H) and ileum (not shown) after *S. typhimurium* infection. Taken together, these data indicate that NcDase is necessary to mount an effective IFN-γ immune response to enteric bacterial infections.

NcDase is crucial in innate immunity against *C. rodentium*

To test whether innate immune cells were responsible for the induction of IFN-γ-producing T cells in the gut, we further characterized the myeloid cell composition and cytokine profile of *C. rodentium*-infected mice by CyTOF and FACS analysis. We observed a substantial increase in CD11b^{+} DCs (Figure S4A cluster 3), inflammatory Ly6C^{hi} monocytes (Figures S4A cluster 5 and S4B), and CD206^{+} M2-like macrophages (Figure S4A cluster 8), in NcDase$^{-/-}$ mice after colonization. However, changes in myeloid cell composition were associated with profoundly decreased production of IL-1β in activated macrophages (Figures S4A cluster 1 and S4D), but similar levels of IL-12 and IL-6 in macrophages and DCs (Figures S4C and S4D). Moreover, reduced migratory CD103^{+} DCs and increased myeloid CD11b^{+} CD103^{-}DCs were found in the colonic mucosa (Figures S4A cluster 2 and S4E), in line with their superior ability to migrate to the mesenteric draining lymph nodes (MLNs) in response to inflammatory signals (Bogunovic et al., 2009).

To further examine the functions of NcDase in innate versus adaptive immunity in infection, we deleted NcDase in recombination activating gene-1 (Rag1)-deficient mice (Rag1$^{-/-}$ NcDase$^{-/-}$). Rag1$^{-/-}$ mice and Rag1$^{-/-}$NcDase$^{-/-}$ mice were then infected by *C. rodentium*. Rag1$^{-/-}$ mice gradually lost weight and eventually became moribund or died around day 30, owing to their lack of T and B cells and thus their inability to mount antibody responses to *C. rodentium* (Zheng et al., 2008). In contrast, most of the Rag1$^{-/-}$NcDase$^{-/-}$ mice lost more body weight (Figure 3A) or died sooner, i.e., during the first 3 weeks of infection (Figure 3B). Consistent with this observation, Rag1$^{-/-}$NcDase$^{-/-}$ mice showed severe colonic inflammation and liver necrosis and inflammation (Figures 3C and 3D), increased bacterial burden in the feces (Figure 3E) and dissemination to peripheral organs (Figure 3F), and decreased secretion of intestinal IL-1β (Figure 3G) and NcDase metabolite sphingosine (SPH) (Figure 3H) compared with Rag1$^{-/-}$ mice. To assess the role of macrophages, infected mice were injected with clodronate liposomes (Figure S5A). Interestingly, all Rag1$^{-/-}$NcDase$^{-/-}$ mice and Rag1$^{-/-}$ mice treated with clodronate for depletion of macrophages died at a similar time point after infection (Figure S5B). Also, macrophage depletion led to bacterial shedding and fecal lipocalin-2 production in Rag1$^{-/-}$ mice to levels similar to those of macrophage-depleted Rag1$^{-/-}$NcDase$^{-/-}$ mice (Figures S5C and S5D). Taken together, our data demonstrate that the interaction of macrophages and NcDase metabolite sphingosine might be essential for protecting mice from death during the *C. rodentium* infection in the absence of adaptive immunity.

NcDase in intestinal macrophages is required for initiating adaptive immune responses

Intestinal macrophages are required for T cell polarization in response to *C. rodentium* (Schreiber et al., 2013). For example, CD103^{-}CD11b^{+}F4/80^{+} macrophages located in the lamina propria and the serosa normally express IL-10 and other anti-inflammatory cytokines (Denning et al., 2007; Rivollier et al., 2012) but can produce pro-inflammatory cytokines

such as IL-12 in response to infection (Kim et al., 2011; Rivollier et al., 2012). Although the increase in $CD11c^{low}MHCII^{-}CD11b^{+}F4/80^{+}$ macrophages was observed in $NcDase^{-/-}$ (Figures 1B and S4), how macrophage-derived anti-inflammatory or pro-inflammatory cytokines contribute to adaptive responses *in vivo* needs to be determined. To determine if NcDase participates in intestinal innate immunity by producing IL-1β and IL-18 that direct T cell polarization (priming), carboxyfluorescein succinimidyl ester (CSFE)-labeled OVA-specific transgenic CD8 T cells (OT-I cells) were injected intravenously (i.v.) into recipient $Rag1^{-/-}$ $NcDase^{-/-}$ or $Rag1^{-/-}$ mice and recipients were orally immunized with OVA. Three days later, after oral gavage of OVA, OT-I cell numbers in the MLN of $Rag1^{-/-}$ $NcDase^{-/-}$ were found to be lower than in WT mice, and these cells had undergone fewer divisions (Figures 4A and 4B). We also assessed whether effector T cells primed in $Rag1^{-/-}$ $NcDase^{-/-}$ mice were capable of localizing to the SI epithelium and lamina propria 3 days later. OT-I cells primed in $Rag1^{-/-}NcDase^{-/-}$ mice displayed significantly reduced divisions and ability to mobilize to the SI (Figures 4A and 4B). Consistently, PBS-treated bone-marrow-derived macrophage (BMDM) and *C. rodentium*-stimulated BMDMs from $NcDase^{-/-}$ mice, but not LPS-derived BMDMs, displayed a significantly decreased ability to affect the proliferation (Figure 4C) and activation of effector $CD4^{+}$ T cells *in vitro* (Figure 4D). Collectively, these results demonstrated that NcDase determined the capacity of macrophages for the induction of T cell priming and IFN-γ production, in line with the defective IFN-γ^{+} T cells in the gut of $NcDase^{-/-}$ mice.

NcDase and sphingosine are important in bacteria killing and control bacteria-induced inflammasome activation and IL-1β expression by macrophages

Functionally, NcDase converts ceramide into sphingosine. We next examined the levels of sphingosine and NcDase activity during *C. rodentium* infection. *C. rodentium* infection leads to decreases in NcDase activity (Figure 5A) and sphingosine release (Figure 5B) in the colon. Interestingly, our studies further revealed that the NcDase appeared to be predominantly carried by luminal extracellular vesicles (EVs) rather than gut tissue in WT mice (Figure 5C). Furthermore, NcDase activity in the luminal EVs was also strongly suppressed by *C. rodentium* infection (Figure S6A). We next sought to study how NcDase deficiency promotes the infection of *C. rodentium*. First, we found sphingosine has direct bactericidal effects on the growth of *C. rodentium*, consistent with sphingosine exhibiting antimicrobial properties against pathogenic bacteria (Grassme et al., 2017) (Figure S6B). In addition, phagocytosis and bacterial killing were greatly impaired in BMDMs lacking NcDase compared with WT macrophages (Figures 5D–5F). We considered that the enhancement of the metabolite sphingosine might be the reason for bacterial protection in WT macrophages against *C. rodentium*. To test this hypothesis, we treated macrophages with recombinant NcDase protein, EV-associated NcDase, sphingosine, and sphingosine kinase inhibitor (SKI-178), which are all involved in the sphingolipid pathway and could enhance sphingosine levels. All of these treatments, particularly sphingosine, strongly enhanced phagocytosis and suppressed propagation of *C. rodentium* (Figures 5D–5F).

Our *in vivo* results showed that NcDase deletion increased sensitivity to bacterial infection and lowered IL-1β production. IL-1β secretion in response to bacteria or endotoxin requires caspase-1 activation, which cleaves pro-IL-1β into its active mature secreted form. We next

tested the role of NcDase in IL-1β expression and inflammasome activation in macrophages in response to bacterial challenge. Macrophages lacking NcDase expression showed significant reduction in cleaved IL-1β and expressed lower p10 caspase 1 compared with the WT macrophage (Figures 5G and 5H) response to *C. rodentium* infection as measured by immunoblotting and ELISA. The effects on IL-1β were specific, as bacterial exposure induced a robust increase in TNF-α that was independent of NcDase (Figure 5H). Moreover, WT macrophages showed a response to the sphingosine, SKI-178, NcDase protein, and NcDase^{+} EV treatment with significantly greater IL-1β expression and caspase-1 activation compared with control treatment (Figures 5I, 5J, S6C and S6D), so presumably all of these increase the endogenous sphingosine. Taken together, we concluded that sphingosine, which is produced by soluble NcDase or EV-associated NcDase, is antibacterially active and may have an immunomodulatory function that is required for bacterial clearance in macrophages.

NcDase serves as a metabolic switch for macrophage inflammasome activation

We next investigated the underlying molecular mechanism by which NcDase regulates inflammasome activation. Macrophage activation and function are controlled by cellular metabolism, and M1-like macrophages predominately use aerobic glycolysis as an energy source (Divakaruni et al., 2018). To determine whether NcDase regulates aerobic glycolysis, we conducted a glycolysis stress test to WT and NcDase$^{-/-}$ BMDMs that had been treated *in vitro* with control (M0), LPS + IFN-γ (M1), or ceramide for 17 h. We measured the extracellular acidification rate (ECAR) using Seahorse assay, which quantifies proton production as a surrogate for lactate production and thus reflects overall glycolytic flux. Deficiency of NcDase in M0 BMDMs and M1 BMDMs significantly decreased the basal ECAR level and decreased glycolytic reserve capacity (Figure 6A). Notably, ceramide treatment in WT macrophages increased the ECAR and glycolytic capacity to control treatment, while ceramide treatment in NcDase$^{-/-}$ cells did not increase the ECAR any further (Figure 6B). Because ceramide preferentially targets autophagosomes to mitochondria, we also examined whether NcDase deficiency or ceramide accumulation alters mitochondrial function by measuring the oxygen consumption rate (OCR). Ceramide treatment slightly reduced the OCR compared with control treatment in WT macrophages. Treatment of NcDase-deficient macrophages with ceramide did not inhibit OCR but increased OCR compared with vehicle (control) treatment (Figure 6C), possibly because ceramide degradation results in a higher level of sphingosine in WT macrophages but not in NcDase-deficient cells. Importantly, sphingosine treatment increased the ECAR, glycolytic reserve, and capacity to control treatment not only in WT macrophages but also in NcDase$^{-/-}$ macrophages (Figure 6D). Furthermore, SPH treatment greatly enhances LPS-induced glycolytic capacity (Figure 6E), consistent with the results that SPH serves as second signal for IL-1β production in LPS-primed macrophages. Thus, these data indicate that sphingosine regulates glycolytic metabolism in macrophage. We next examined if there are changes in gene expression of enzymes of the glycolytic pathway in macrophages after sphingosine treatment. Quantitative PCR analysis of the different glycolytic genes showed 3-to 4-fold increase in both hexokinase (Hk2) and glucose-6-phosphate isomerase (Gpi) expression, enzymes that catalyze the phosphorylation of glucose to hexose 6-phosphate and the conversion of glucose-6-phosphate to fructose-6-phosphate in the glycolytic pathway, respectively (Figure 6F). SPH treatment also results in a 2- to 3-fold increase

in expression of enzymes Pgam1 and Ldha (Figure 6F) in both types of macrophages, suggesting that exogenous sphingosine can compensate for the decreased glycolysis in NcDase$^{-/-}$ macrophages. Ceramide and sphingosine are known to regulate the activity of the phosphatase PP2A, which plays a critical role in dephosphorylation and activation of the NLRP3 inflammasome (Stutz et al., 2017). To explore whether NcDase-induced caspase-1 activation occurred via PP2A, we treated macrophages with the PP2A serine/threonine phosphatase inhibitor okadaic acid (OA) just prior to incubation with sphingosine. OA significantly decreased sphingosine-induced IL-1β release (Figure 6G). Consistent with this, we found a significantly lower level and reduced activity of PP2A in the colon of NcDase$^{-/-}$ mice compared with WT mice after *C. rodentium* infection (Figures 6H and 6I). Notably, NcDase-deficient colonic macrophages had reduced glycolytic reserve capacity compared with WT colonic macrophages isolated from infected mice (Figure 6J). Importantly, inhibition of glycolysis by 2-deoxyglucose (2-DG) reduced sphingosine-induced IL-1β release and PP2A activity (Figures 6K and 6L) in macrophages. Taken together, these data suggest that sphingosine-induced glycolysis targets the inflammasome machinery through the activation of PP2A.

Administration of a high-sphingomyelin diet or inhibition of SphK1 prevents pathogen colonization in the gut

Because sphingomyelinase and ceramidase may generate bioactive sphingosine from dietary and endogenous sphingomyelin, we examined the levels of the key metabolites sphingomyelin and ceramide species during *C. rodentium* infection (Figure S7A). The analysis revealed that *C. rodentium* infection leads to a decrease in total sphingomyelin and specific sphingomyelin with very-long-chain fatty acids ($C_{20:0}$, $C_{22:0}$, $C_{24:0}$, and $C_{24:1}$) in the colon (Figure S7B). However, the total and specific acylchain ceramides ($C_{22:0}$, $C_{24:0}$, and $C_{24:1}$) (Figure S7C) and the S1p were increased significantly in the colon (Figure S7D). These results suggest that *C. rodentium* lowers the level of sphingomyelin and limits the production of sphingosine by inhibiting the activity of NcDase or by increasing the activity of SphK1 in the gut. Digestion of dietary sphingomyelin (SM) in the intestine yields ceramide and sphingosine that can be absorbed into intestinal mucosal cells. We thus hypothesized that increased amounts of dietary SM or endogenous sphingosine may influence *C. rodentium* colonization in the gut. To test this, we fed C57BL/6J mice with 0.25% of an SM diet calculated by weight (12.5 mg/mouse/day) every day starting 1 week prior to pathogen inoculation. We found that mice treated with 12.5 mg of the SM diet per day and inoculated with 2×10^9 colony-forming units (CFU) of *C. rodentium* showed approximately a 3-log lower pathogen load on day 7 post infection compared with control mice (Figure 7A). Notably, these differences in pathogen colonization were mainly observed at and after the peak of pathogen expansion or during the eradication phase (Figure 7A). Consistently, there was reduced fecal lipocalin-2 for gut inflammation, lower colonic pathology (Figures 7B and 7C), increased IFN-γ secretion in the colon and ileum tissue (Figure 7D), and a higher percentage of CD8αβ$^+$ T cells, Th1 cells (Figure 7E), and IFN-γ$^+$CD8$^+$ T cells (Figure S7E) in the LPLs of mice treated with SM. Since the increased activity of SphK1 promotes the phosphorylation of sphingosine to form sphingosine 1-phosphate, we wonder whether deletion or inhibition of SphK1 to increase endogenous sphingosine is sufficient to prevent pathogen colonization. Of note, mice treated

with the SphK1 inhibitor SKI-178 not only showed decreased pathogen levels but also lowered gut inflammation compared with the control group (Figures 7A–7C). The protection is correlated with increased levels of IFN-γ and IFN-γ^+ T cells (Figures 7D, 7E, and S7E). Likewise, genetic deletion of SphK1 resulted in protection of the mice against oral pathogen challenge, which correlated with reduced fecal lipocalin-2 in feces and lower intestinal pathology scores compared with WT mice (Figures 7F–7H). We further found that a marked increase in the activity of NcDase and the amounts of sphingosine in the ileum and a modest increase in sphingosine in the colon of mice treated with the high-milk SM diet or SKI-178 compared with control animals (Figures S7F and S7G). These experiments suggest that increases in sphingosine and Th1 cells could explain the immune-response-dependent protective effects of dietary sphingomyelin in the context of *C. rodentium*-induced colitis.

DISCUSSION

Our findings highlight an intestine-intrinsic regulation between sphingolipid metabolites and gut nutritional immunity against a mucosal pathogen. Specifically, we identified that the NcDase metabolite sphingosine is necessary to induce innate and adaptive responses to initiate defense against the enteric *C. rodentium* infection.

Our findings revealed that NcDase deficiency underlies the defects in intestinal T cell homeostasis. We found that NcDase$^{-/-}$ mice in steady state have significantly reduced numbers of CD8αβ$^+$ T cells, Th1 cells, and CD8αβ$^+$ IFN-γ^+ T cells in the intestine. Our results further showed that CD103$^-$CD11c$^+$CD11b$^+$ F4/80$^+$ macrophages produced lower levels of IL-1β in NcDase$^{-/-}$ mice after *C. rodentium* infection, supporting the idea that intestinal macrophage is essential for an optimal Th1 response to *C. rodentium* (Schreiber et al., 2013). These are consistent with the notion that myeloid IL-18 or IL-1β production may synergize with IL-12 to maintain optimal IFN-γ responses (Freeman et al., 2012). The adaptive immune response to *C. rodentium* is characterized by the recruitment of Th1, Th22, and Th17 cells (Geddes et al., 2011; Mullineaux-Sanders et al., 2019). Our study indicates that NcDase likely contributes to adaptive Th1 immunity via innate immune cells in *C. rodentium*-induced colitis. However, since Th17 cells induced by *C. rodentium* can generate a vigorous inflammatory response, we cannot exclude that increased Th17 cells in infected NcDase$^{-/-}$ mice also accelerate the damage of gut. Further experiments need to investigate the role of NcDase in the regulation of gut Th17 cells.

Next, we generated and infected Rag1$^{-/-}$NcDase$^{-/-}$ mice to differentiate NcDase function between adaptive immunity and innate immunity. Rag1$^{-/-}$NcDase$^{-/-}$ mice had more weight loss and earlier mortality than Rag1$^{-/-}$ mice in *C. rodentium*-induced colitis. Clodronate treatment of Rag1$^{-/-}$ and Rag1$^{-/-}$NcDase$^{-/-}$ mice infected with *C. rodentium* led to comparable bacterial load and mortality. These experiments demonstrate that the majority of the sphingosine pathway is still intact in Rag1$^{-/-}$ mice and NcDase-mediated innate immunity does play a role during the *C. rodentium* infection. The role of intestinal macrophages in the adaptive immune response has been difficult to define, in part because of their ability to produce anti- or pro-inflammatory cytokines under different physiological and pathological conditions (Gordon and Taylor, 2005). Our *in vivo* experiments based on transferring OT-I T cells and macrophage OT-II cells *in vitro* in coculture experiments

revealed that NcDase is essential for intestinal macrophage-induced Th1 polarization, highlighting that intestinal macrophages are required for T cell polarization in response to *C. rodentium* infection (Schreiber et al., 2013). Thus, our results illustrate that the functional importance of NcDase is associated with sphingosine production and the ability of the macrophages to evoke an archetypical bacterial clearance response. Although NcDase is more highly expressed in the gut, more in-depth mechanistic approaches, including studies in mice with macrophage/IEC-specific deletion of NcDase, will be required to fully understand the mechanism of enteric infection.

Sphingosine has been shown to exhibit antimicrobial properties against pathogenic bacteria and virus, such as *Pseudomonas aeruginosa* (Grassme et al., 2017) and herpes simplex virus (Lang et al., 2020). Our studies demonstrate a critical role of sphingosine that enhances bactericidal function *in vitro* and *in vivo*. First, we found that sphingosine can directly inhibit *C. rodentium* growth. Furthermore, we have discovered that NcDase/sphingosine can act as a bioactive lipid danger-associated molecular pattern (DAMP) signal and can induce inflammasome-dependent activation of caspase-1 and secretion of mature IL-1β. Inflammasome-dependent processing of IL-1β and IL-18, and the inflammasome sensors NLRP3, NLRC4, ASC, and caspase 1 are all required for *C. rodentium* clearance (Mullineaux-Sanders et al., 2019). We also have shown that enhancement of sphingosine production can occur by the addition of NcDase protein and SphK1 inhibitor-induced IL-1β secretion and inflammasome activation in macrophages.

Glycolysis is a critical pathway in cellular glucose metabolism that provides intermediates for energy generation. Glycolysis in M1 macrophages is well known to be critically required for inflammasome activation and IL-1β production (Moon et al., 2015; Tannahill et al., 2013; Xie et al., 2016). Our data suggest that sphingosine controls macrophage phenotype through metabolic reprogramming, as sphingosine regulates several key enzymes such as Hk2, Gpi, Pgam1, and Ldha in the glycolytic pathway. Production of reactive oxygen species (ROS) regulated by hexokinase (Hk2) was suggested to be important for glycolysis-dependent NLRP3 inflammasome activation (Moon et al., 2015). Both sphingosine and ceramide are known to activate PP2A (Habrukowich et al., 2010; Oaks and Ogretmen, 2015), which is critical for NLRP3 activation (Habrukowich et al., 2010; Stutz et al., 2017). We have shown that inhibition of glycolysis by 2-DG markedly suppressed the PP2A activity and inflammasome-mediated caspase-1 activation in response to LPS and sphingosine. Our results suggest that a glycolysis-dependent PP2A signal was important for sphingosine-induced inflammasome activation. The impairment in the macrophage response in NcDase$^{-/-}$ mice is driven by defective IL-1β processing via the inflammasome/caspase-1 pathway, revealing an unsuspected mechanism by which macrophages using sphingosine sense the pathogens. Thus, the combination of antimicrobial and immunomodulatory activities may suggest that sphingosine could be an important bioactive lipid factor for pathogen clearance.

Deciphering the complex interactions between the gut immune cells, diet, and colitis remains a major challenge in the development of diet-based therapies for the prevention and treatment of infectious colitis. Sphingomyelin is a major polar milk lipid and is degraded in the intestine to metabolites (ceramide, sphingosine, and S1p) that affect mucosal growth

and immune maturation (Meiners et al., 2019; Norris et al., 2016b). A previous human study showed that significant levels of both sphingomyelinase and NcDase were found in meconium from both preterm and term infants (Duan et al., 2007). Interestingly, we found that the gut luminal EVs have stronger NcDase activity than gut tissue, indicating that NcDase is mainly carried by luminal EVs for dietary sphingolipid digestion. *C. rodentium* colonizing the distal SI and colon may inhibit sphingosine production and induce S1p biosynthesis. Our results showed that mice fed with a high-sphingomyelin diet exhibited a reduction of *C. rodentium* colonization, which was associated with a marked increase in NcDase activity and sphingosine production in the ileum and colon. Consistently, deletion or inhibition of SphK1 can prevent the *C. rodentium*-induced colitis, probably through increasing the sphingosine stability and reducing the generation of S1p. Our data demonstrate that the influence of dietary sphingomyelin on enteric infections involves numerous potentially additive or offsetting effects between sphingolipid metabolites and the gut immune cells that should be considered when developing specific diets in the clinic. The current study may help in designing new strategies to prevent or treat enteric infections by targeting metabolic pathways, such as sphingolipid metabolites, through dietary or other types of interventions.

Limitations of the study

In this study, we have identified the role of NcDase and its metabolite sphingosine in driving mucosal IFN-γ^+ T cell responses and regulating glycolysis and IL-1β production in macrophages. BM chimera experiments further demonstrated NcDase is T cell extrinsic. Nevertheless, NcDase is highly expressed at the IECs, and IECs can modulate the function of host immune cells. For example, TCR$\alpha\beta^+$ IELs do not respond to conventional major histocompatibility complex (MHC)-peptide ligands but to ligands expressed abundantly on IECs, such as the thymus leukemia antigen ligand for CD8$\alpha\alpha^+$ IELs (Leishman et al., 2001). We therefore cannot exclude that IFN-γ^+ T cell responses are mediated by the expression of immune receptors, and the secretion of cytokines and chemokines from the IEC basolateral side. Furthermore, it is not clear how to link macrophage glycolysis with Th1 responses to bacterial infection *in vivo*. The molecular and cellular mechanisms of sphingosine-mediated glycolysis remain to be elucidated. Finally, we presently do not know about the human relevance of our findings, since our work was primarily conducted in mice *in vitro*.

STAR ★METHODS

RESOURCE AVAILABILITY

Lead contact—Further information and requests for resources and/or reagents should be directed to and will be fulfilled by Dr. Zhongbin Deng (zhongbin.deng@louisville.edu).

Materials availability—Materials generated in this study are available from the lead contact.

Data and code availability

- All data reported in this paper will be shared by the lead contact upon request.

- This paper does not report any original code.
- Any additional information required to reanalyze the data reporting in this paper is available from the lead author on request.

EXPERIMENTAL MODEL AND SUBJECT DETAILS

Mice—C57BL/6 mice, C57BL/6 (CD45.1) mice and Rag1-deficient mice ($Rag1^{-/-}$) were obtained from Jackson Laboratory. NcDase knockout mice ($NcDase^{-/-}$) were from Dr. Yusuf A. Hannun (Stony Brook University) and had been backcrossed at least 8 generations to C57BL/6 (Kono et al., 2006). $NcDase^{-/-}$ and $Rag1^{-/-}$ mice were crossed to generate $Rag1^{-/-}NcDase^{-/-}$ mice. For infections experiments, we used age- and sex-matched mice between 10 and 14 weeks of age. Both female and male WT littermates and $NcDase^{-/-}$ mice were used in all of experiments. Studies were approved by the University of Louisville Institutional Animal Care and Use Committee.

C. rodentium and *S. Tm* infection—Mice were infected orally with 2×10^9 CFU *C. rodentium* strain DBS100 (ATCC 51459) in a total volume of 100 μL. Bacterial numbers in feces and homogenized tissues were determined by plating serial dilutions onto MacConkey agar. Colony-forming units (CFUs) were counted and normalized to stool weight after 24 h. For ODN-BW006 (Invivogen) treatment, 10 μg ODN-BW006 per mouse was injected on day 3 and 5 post-infection. For milk sphingomyelin treatment (Avanti Polar Lipids), mice were orally given 12.5 mg per day one week before infection and maintained every day after infection. The amount (12.5 mg per day) of dietary milk sphingomyelin calculated based on the 0.25% sphingomyelin diets, which was equivalent to 22 mg/kg of body weight in a human or roughly 1.5 g/day to a 70-kg human, based on body surface normalization (Norris et al., 2016a). For SKI-178 treatment, mice were treated with SKI-178 (10 mg/kg) i.p. every two days thereafter during the 15 days of the experimental period. Some mice were sacrificed between day 7 and 10 after infection to determine pathogen loads in the liver and spleen, and to process colonic tissues for Hemotoxylin and Eosin (H&E) staining, whereas the rest of the mice were used to monitor mouse survival. For *S.Tm* infection, water and food were withdrawn for 4 h before mice were treated with 20 mg/mouse of streptomycin by oral gavage (o.g.). Afterward, mice were supplied with water and food ad libitum. Twenty hr after streptomycin treatment, water and food were withdrawn again 4 h before the mice were infected with 10^5 CFU of *S. Tm* (ATCC,14028) in 200 mL PBS. Drinking water ad libitum was supplied immediately and food 2 h post infection (p.i.). Mice were weighted every day and survival was monitored.

METHOD DETAILS

Time-of-flight mass cytometry (CyTOF) experiments—Single cell suspensions of intestinal mononuclear cells were centrifuged at 350 × g at 4°C for 5 min and the supernatant removed by aspiration. Cells were resuspended in 1 mL CyTOF staining buffer (CFB - PBS containing 0.1% BSA, 2 mM EDTA and 0.05% sodium azide) and washed in CFB a second time. Primary antibody staining was performed and diluted in CFB, for 40 min on ice. Cells from individual samples were bar-coded with anti-CD45 antibodies, pooled and stained with the following antibodies: Ly6G (141 Pr), CD11c (142 Nd), CD8

(168Er), CD11b (172Yb), CD19 (149 Sm), CD25 (151 Eu), F4/80 (146 Nd), CD36 (147 Sm), CD3e (152 Sm), CD274 (153Eu), CD62L (160 Gd), CD73 (154 Sm), Ly6c (150Nd), Cx3cr1 (164 Dy), CD103 (163 Dy), CD206 (169 Tm), NK1.1 (170 Er), CD44 (162Dy), CD4 (145Nd), MHCII (209Bi), B220 (176 Yb). A mixture of pre-conjugated (Fluidigm) and in house conjugated (using Maxpar X8 labeling kits – Fluidigm) was used. Following primary antibody staining, cells were washed as described previously using 1 mL CFB and resuspended in 0.5 mL of a 1/4000 dilution of cisplatin viability reagent (Cell-ID Cisplatin-Fluidigm, Ca) in PBS for 5 min at room temperature. Cisplatin staining was terminated by addition of 1 mL of CFB and cells were washed twice by centrifugation. Next, cells were resuspended in 400 μL of 4% paraformaldehyde in PBS (PFA) and fixed at room temperature (RT) for 20 min, then washed twice by centrifugation with 1 mL CFB. Samples were acquired with a Helios Mass Cytometer (Fluidigm, South San Francisco, CA) and data were plotted using tSNE or UMAP analysis. Gates were done as described in Results section.

Macrophage depletion, and T cell transfers—For tissue macrophage depletion, $Rag1^{-/-}$mice and $Rag1^{-/-}NcDase^{-/-}$ mice were injected intravenously with 200 μL of clodronate liposomes (Encapsula Nanosciences) at day −2, 0, 2, and 4 after C. rodentium infection. For T cell transfers, naive OT-I cells were labeled with CellTrace CFSE (Life Technologies) according to the manufacturer's instructions and injected i.v. (3×10^6 cells/mouse) into $Rag1^{-/-}$ mice and $Rag1^{-/-}NcDase^{-/-}$ recipient mice. OT-I recipients were then immunized by oral gavage with OVA (50 mg, Grade V, SigmaAldrich). OT-I recipients were sacrificed 1–3 days after immunization.

Bone marrow chimera mice—To generate BM chimeric mice, WT recipients (45.2) received a single lethal total body irradiation dose of 9 Gy. On the following day, 5×10^6 mixed or single BM cells from $NcDase^{-/-}$ mice (45.2) or WT mice (45.1) were injected i.v. into the WT mice (45.2) and then rested for 8 weeks before use.

Cell culture—BMDMs were generated in the presence of L-929 conditional medium. After pretreatment with ultrapure LPS (200 ng/mL) for 3 h to induce pro-IL-1β expression, BMDM were stimulated with BSA alone or EVs (30 μg-200 μg) for 3 h, Sphingosine (25 μM,1 h), SKI-178 (100 μM) for 3 h, or C. rodentium (MOI = 10) for 7 h, as indicated. Where indicated, chemical inhibitors were added 30 min before cell stimulation (2.5 h after LPS priming). Supernatant and cell lysate were collected for ELISA and Western blot analysis. For T cells proliferation, BMDMs(2×10^5 or 5×10^5, respectively) were co-cultured with FACS-sorted Celltrace CFSE-labeled naive $CD8^+$ OT-I (1×10^5), or $CD4^+$ OT-II cells and chicken ovalbumin (10 μg/mL, Grade VI, Sigma-Aldrich) in 200 μL RPMI complete medium in 96-well round-bottom plates. Some BMDM were stimulated by LPS for 3 h or loaded previously with *C. rodentium* at a 10:1 ratio, in the presence of 100 U/mL penicillin, 100 μg/mL streptomycin and 50 μg/mL gentamycin. After 24 h–72 h, cell proliferation was analyzed by Celltrace CFSE dilution (flow cytometry) and supernatants assessed for IFN-γ quantification by ELISA. For nonpolarizing (Th0) conditions, naive cells were stimulated with anti-CD3 (2C11; Bio X Cell), anti-CD28 (37.51; Bio X Cell) and

IL-2 (100 U/mL); for Th1 conditions, naive cells were cultured with IL-12 (0.5 ng/mL) and anti-IL-4 (10 μg/mL; 11B11; Bio X Cell).

Oxygen-consumption rate and extracellular acidification rate—Bone-marrow-derived macrophages (BMDMs) or macrophages sorted from colonic LPLs were plated in XF-96 cell culture plates (6.5×10^5 cells/well) and polarized for 17 h toward M1 with IFN-γ (50 ng/mL) plus LPS (100 ng/mL), treated with ceramide (20 μM) for 17 h, or treated with sphingosine (25 μM) for 3 h, respectively. Macrophages were then washed and incubated for 1 h in XF assay medium (unbuffered DMEM pH 7.4 with 2 mM L-glutamine and 10 mM glucose and 2 mM sodium pyruvate for oxygen consumption rate (OCR) or without glucose and pyruvate for extracellular acidification rate (ECAR) in glycolysis stress test in a non-CO_2 incubator at 37°C as per manufacturer's instructions (Seahorse Bioscience). Real-time measurements of macrophage extracellular acidification rate (ECAR) and oxygen consumption rate (OCR) were performed using an XF-96 Extracellular Flux Analyzer (Seahorse Bioscience). Three or more consecutive measurements were obtained under basal conditions and after the sequential addition of 1.5 μM oligomycin, to inhibit mitochondrial ATP synthase; 1.5 μM FCCP (fluoro-carbonyl cyanide phenylhydrazone), a protonophore that uncouples ATP synthesis from oxygen consumption by the electron-transport chain; and 0.5 μM rotenone plus 0.5 μM antimycin A, which inhibits the electron transport chain. To assess glycolysis, three or more consecutive ECAR measurements were obtained under basal conditions and after the sequential addition of 1.5 μM oligomycin, to elicit maximal glycolytic capacity and 50 mM 2-DG (2-deoxyglucose) to inhibit glycolysis-dependent ECAR.

Sphingolipid analysis—Ceramide species, sphingosine and S1p from gut of mice were collected and analyzed with LC-MS/MS by the Lipidomics/Metabolomics Shared Resource (Virginia Commonwealth University), as we previously reported (Gu et al., 2021). In brief, calibration curves were constructed by plotting peak area ratios of synthetic standards corresponding to each target analyte with respect to the appropriate internal standard. The target analyte peak areas from the samples were similarly normalized to their respective internal standard and then compared with the calibration curves using a linear regression model. Results were normalized to total protein levels. In some experiments, Sphingosine was also analyzed by ELISA Kits (Aviva Systems Biology).

Survival experiments—To analyze the effect of macrophage/sphingosine deficiency on the course of infection, we performed survival experiments. Animals were checked daily, sacrificed with corresponding termination criteria, and counted as dead. Termination criteria were body weight, general condition, spontaneous behavior, and clinical findings.

Isolation of gut extracellular vesicles—Isolation of gut EVs was performed as described previously (Deng et al., 2015). Briefly, mice were euthanized and the intestine removed. The luminal contents of the intestine were removed by gently flushing the intestine with ice-cold PBS. The intestine was then opened longitudinally and gently washed with ice-cold PBS. The mucous was scraped off by mild physical separation using a glass slide, soaked in washing PBS, agitated on a rotator at 70 r.p.m. min^{-1} for 15 min and

centrifuged at 500×*g* for 15 min at 4°C. The supernatant was then followed by differential centrifugation: 4000 rpm for 30 min, 8000 rpm for 60 min, 36000 rpm for 90 min. The pellets from the 8000 rpm or 36000 rpm centrifugations were used for microparticles and exosome-like particles, respectively. Protein concentration was determined using the Bio-Rad Protein Quantitation Assay kit with BSA as a standard.

Assay of ceramidase activity—The neutral ceramidase activity was measured using C12 NBD Ceramide (d18:1/12:0) (Caymanchem) as the substrates. Small and large intestine were harvested after mice were fasted for 18 h. Mucosa was obtained by cutting the entire small intestine longitudinally and scraping the mucosa off with a glass slide. Gut Mucosa and liver were homogenized in RIPA buffer with protease inhibitor mixture (Sigma-Aldrich) and centrifuged at 10,000×g at 4°C for 15 min 30–50 μg of homogenate protein in the supernatant was incubated in 100 μL of reaction buffer (25 mM Tris-HCI, pH 7.5, 1% sodium cholate, and 50 μM NBD C_{12}-ceramide) at 37°C for 2.5–3 h. The reaction was terminated by the addition of 300 μL of chloroform/methanol (2/1, v/v). This solution was vortexed and centrifuged at 8,000×g for 1 min. The lower layer was dried in a SpeedVac concentrator, dissolved in 10 μL of chloroform/methanol (1/1, v/v), and applied onto TLC plates (silica gel, Sigma). The TLC was developed with chloroform/methanol/2.5 N ammonia (90/30/0.5, v/v/v). Ceramide and fatty acid were separated by TLC and quantitated using a fluorescent image analyzer.

Histology and immunofluorescence—Tissue specimens were fixed in 10% formalin, dehydrated, and then embedded in paraffin. Tissue samples were cut at 5 mm thicknesses and stained with hematoxylin and eosin. Sections were scanned using an Aperio Imagescope. For immunofluorescence analysis, OCT (Sakura Finetek)-embedded tissue cryosections (6 μm-thick) were blocked for 1 h at 22°C with 5% BSA in PBS and incubated overnight at 4°C with the primary antibodies, i.e., F4/80 (BM8), EpCAM (eBioscience, ThermoFisher), rabbit polyclonal IL-1β (Abcam) or anti-sphingosine antibody (Antibody Research Corporation, #111334). Primary antibodies were detected by Alexa Fluor 488, 594 or 647 conjugated goat anti-mouse, anti-rabbit IgG and anti-rat (1:600, Invitrogen). Tissues were counterstained with DAPI and images were captured on a Zeiss LSM 510 confocal microscope equipped with a digital image analysis system (Pixera).

Histological scoring—The pathology score was evaluated blindly by one pathologist using a scoring system. Briefly, severity of inflammation (0 = none, 1 = mild, 2 = moderate, 3 = severe), level of involvement (0 = none, 1 = mucosa, 2 = mucosa and submucosa, 3 = transmural), and extent of epithelial/crypt damage (0 = none, 1 = basal 1/3, 2 = basal 2/3, 3 = crypt loss, 4 = crypt and surface epithelial destruction) were determined. Each variable was then multiplied by a factor reflecting the percentage of the cecum/colon involved (0–25%, 26–50%, 51–75%, 76–100%), and then summed to obtain the overall inflammation score for each sample of 0–8.

Reagents, antibodies and flow cytometry—D-erythro-Sphingosine, A740003, Sphingosine, SKI-178 and PP2A assay Kits were purchased from Sigma-Aldrich. For analysis of surface markers, cells were stained in PBS containing 2% (wt/vol) BSA.

Intracellular staining of the transcription factors Foxp3 was performed using the Foxp3 Fix/Perm Buffer Set (eBioscience, Thermo fisher). For detection of intracellular cytokines, cells were first stimulated for 4 h with 50 ng/mL PMA and 1 μg/mL ionomycin in the presence of Brefeldin A (5 μg/mL; All obtained from Sigma), followed by staining for surface markers. Cells were then fixed and permeabilized using the Foxp3 Fix/Perm Buffer Set and stained for intracellular cytokines. The following antibodies were used at a dilution of 1/200–1/600: PerCP-Cy5.5, PE-, FITC-or APC-labeled anti-IL-17A (TC11-18H10.1), PE- or APC-labeled anti-IL-4 (11B11, eBioscience, Thermo fisher), PE- or APC-labelled anti-IL-10 (JES5-16E3), APC- or PE-Cy7-labeled anti-IFN-γ (XMG1.2), PE-labeled anti-Foxp3 (FJK-16s, eBioscience, Thermo fisher), PE-, FITC-or APC-labeled anti-CD11b (M1/70), PE-, FITC-or APC-labeled anti-CD4 (RM4-5), PE-Cy7-labeled anti-CD3 (145-2C11), PE-anti-Gr-1 (RB6-8C5), PE-or FITC-labeled anti-mouse Ly6G (1A8), APC-conjugated CD45.2 (104), PE-conjugated anti-CD45.1 (A20), FITC-, PerCP-Cy5.5 or Pacific Blue-labelled anti-CD45 (30-F11), PE-anti-SCA1 (D7), PE-anti-S1PR1 (FAB7089P,R&D). All antibodies were obtained from ThermoFisher unless otherwise noted. Flow cytometry data were acquired on a 5-color FACScan (Becton Dickinson) and analyzed using FlowJo software (Treestar). Cell sorting was performed using a FACSAria II.

Isolation of lamina propria lymphocytes (LPLs) and hepatic immune cells— The method used for isolation of LPLs has been reported previously (Deng et al., 2015). In brief, fat tissues and Peyer's patches (PPs) were removed from small intestine. The intestine was open and cut in pieces 1-cm long and incubated in an HBSS solution containing 5 mM EDTA and 10 mM Hepes for 30 min at 37°C with slow rotation (180 rpm.). Pieces were then cut into smaller pieces and incubated in an HBSS solution containing 0.5 mg mL^{-1} DNase I (Roche) and 1 mg mL^{-1} collagenase type IV (Worthington). Finally, the solution containing digested tissue was passed through a 100-μm cell strainer and LPLs were recovered at the interface of the 40% and 72% Percoll (GE Healthcare) solutions. Livers were perfused with saline solution by way of the portal vein which was followed by enzymatic digestion. Liver immune cells were purified by centrifugation using a Percoll gradient. For flow cytometry analysis, the cells were labeled using standard procedures described above.

ELISA—The quantity of IL-1β, TNF-α, IL-22, and IFN-γ (Thermo Fisher, eBioscience) were determined in culture supernatants, serum, and tissue using ELISA kits according to the manufacturer's instructions. The sensitivity of the assays was <20 pg/mL.

RNA extraction and PCR—Total RNA was isolated from the tissue or lymphocytes of MLNs, small intestine and colon using the Qiagen RNeasy RNA isolation Kit and was used to synthesize cDNA. RNA (1 μg) was reverse-transcribed with Superscript IV and random primers (Invitrogen). For quantitation of genes of interest, cDNA samples were amplified in applied biosystems Realtime System using SYBR Green Master Mix (Invitrogen) and specific primers (Table S1) according to the manufacturer's instructions. Fold changes in mRNA expression between treatments and controls were determined by the δCT method. Results for each sample were normalized to the concentration of GAPDH mRNA or β-actin mRNA (for glycolysis) measured in the same samples and expressed as fold increase over baseline levels, which are set at a value of 1. Differences between groups were determined

using a two-sided Student's t-test and one-way ANOVA. Error bars on plots represent ±SEM, unless otherwise noted. All primers were purchased from Eurofins MWG Operon or Sigma.

Western blot analysis—Tissue or cultured BMDMs were disrupted in RIPA lysis buffer with protease and phosphatase inhibitors (Roche) for 30 min on ice. The samples were centrifuged (16,000 g, 10 min, 4°C) and the resulting supernatants transferred to fresh tubes. Protein lysates were quantitated using a Bio-Rad protein kit (Bio-Rad) and 50–100 μg of lysates were separated on 10% SDS polyacrylamide gels and transferred to a nitrocellulose membrane (Bio-Rad). Appropriate primary antibodies and HRP-conjugated secondary antibodies were used and proteins were detected using the Enhanced Chemiluminescent (ECL) reagent (Thermo Scientific). The images were acquired with ChemiDoc MP System (Bio-Rad).

In vitro bacterial phagocytosis and killing assay—BMDMs were counted using the trypan blue exclusion method, plated at 1×10^6 cells per well in 6-well plates, and grown overnight at 37°C. C. rodentium was labeled by CFSE and added at a multiplicity of infection (MOI) of 1. Chemical inhibitors were added. Bacteria were allowed to bind to cells for 30 min, then DMEM containing 1 μg/mL gentamicin was added to all wells. BMDMs were harvested at indicated time points were washed. For bacterial phagocytosis, BMDMs were digested and stained with (50 μg/mL) ethidium bromide and monitored by confocal microscopy within 2 h. The BMDMs were lysed with H_2O and bacteria were quantified by dilution plating. For the effect of sphingosine on the growth of C. rodentium, C. rodentium were cultured overnight and diluted to an $OD_{600\ nm} = 0.05$ in a 14-mL polystyrene round-bottom tube. Sphingosine or vehicles were then added at a different concentration.

QUANTIFICATION AND STATISTICAL ANALYSIS

Values are shown as Mean ± SEM except where otherwise indicated. t tests were used for continuous variables. The log rank test was used to compare survival differences between different groups. The asterisks indicate significant differences ($p < 0.05$). * indicates $p < 0.05$, **$p < 0.01$, ***$p < 0.001$. n represents the number of independent samples.

Supplementary Material

Refer to Web version on PubMed Central for supplementary material.

ACKNOWLEDGMENTS

This work was supported by grants from the NIH: R21AA025724, R21AI128206, R21AI159194, and R01 DK115406 (Z.D.). We thank Dr. J. Ainsworth for editorial assistance.

REFERENCES

Bogunovic M, Ginhoux F, Helft J, Shang LM, Hashimoto D, Greter M, Liu K, Jakubzick C, Ingersoll MA, Leboeuf M, et al. (2009). Origin of the lamina propria dendritic cell network. Immunity 31, 513–525. [PubMed: 19733489]

Chu S, Sun R, Gu X, Chen L, Liu M, Guo H, Ju S, Vatsalya V, Feng W, McClain CJ, et al. (2021). Inhibition of sphingosine-1-phosphate-induced Th17 cells ameliorates alcoholic steatohepatitis in mice. Hepatology 73, 952–967. [PubMed: 32418220]

Ciorba MA, Bettonville EE, McDonald KG, Metz R, Prendergast GC, Newberry RD, and Stenson WF (2010). Induction of IDO-1 by immunostimulatory DNA limits severity of experimental colitis. J. Immunol 184, 3907–3916. [PubMed: 20181893]

Collins JW, Keeney KM, Crepin VE, Rathinam VAK, Fitzgerald KA, Finlay BB, and Frankel G (2014). Citrobacter rodentium: infection, inflammation and the microbiota. Nat. Rev. Microbiol 12, 612–623. [PubMed: 25088150]

Deng Z, Mu J, Tseng M, Wattenberg B, Zhuang X, Egilmez NK, Wang Q, Zhang L, Norris J, Guo H, et al. (2015). Enterobacteria-secreted particles induce production of exosome-like S1P-containing particles by intestinal epithelium to drive Th17-mediated tumorigenesis. Nat. Commun 6, 6956. [PubMed: 25907800]

Denning TL, Wang YC, Patel SR, Williams IR, and Pulendran B (2007). Lamina propria macrophages and dendritic cells differentially induce regulatory and interleukin 17-producing T cell responses. Nat. Immunol 8, 1086–1094. [PubMed: 17873879]

Divakaruni AS, Hsieh WY, Minarrieta L, Duong TN, Kim KKO, Desousa BR, Andreyev AY, Bowman CE, Caradonna K, Dranka BP, et al. (2018). Etomoxir inhibits macrophage polarization by disrupting CoA homeostasis. Cell Metab. 28, 490–503.e497. [PubMed: 30043752]

Dolowschiak T, Mueller AA, Pisan LJ, Feigelman R, Felmy B, Sellin ME, Namineni S, Nguyen BD, Wotzka SY, Heikenwalder M, et al. (2016). IFN-gamma hinders recovery from mucosal inflammation during antibiotic therapy for Salmonella gut infection. Cell Host Microbe 20, 238–249. [PubMed: 27453483]

Duan RD, Cheng Y, Jonsson BAG, Ohlsson L, Herbst A, Hellstrom-Westas L, and Nilsson A (2007). Human meconium contains significant amounts of alkaline sphingomyelinase, neutral ceramidase, and sphingolipid metabolites. Pediatr. Res 61, 61–66. [PubMed: 17211142]

Duan RD, and Nilsson A (2009). Metabolism of sphingolipids in the gut and its relation to inflammation and cancer development. Prog. Lipid Res 48, 62–72. [PubMed: 19027789]

Freeman BE, Hammarlund E, Raue HP, and Slifka MK (2012). Regulation of innate CD8(+) T-cell activation mediated by cytokines. Proc. Natl. Acad. Sci. U S A 109, 9971–9976. [PubMed: 22665806]

Geddes K, Rubino SJ, Magalhaes JG, Streutker C, Le Bourhis L, Cho JH, Robertson SJ, Kim CJ, Kaul R, Philpott DJ, et al. (2011). Identification of an innate T helper type 17 response to intestinal bacterial pathogens. Nat. Med 17, 837–U202. [PubMed: 21666695]

Gordon S, and Taylor PR (2005). Monocyte and macrophage heterogeneity. Nat. Rev. Immunol 5, 953–964. [PubMed: 16322748]

Grassme H, Henry B, Ziobro R, Becker KA, Riethmuller J, Gardner A, Seitz AP, Steinmann J, Lang S, Ward C, et al. (2017). Beta 1-integrin accumulates in cystic fibrosis luminal airway epithelial membranes and decreases sphingosine, promoting bacterial infections. Cell Host Microbe 21, 707. [PubMed: 28552668]

Gu X, Sun R, Chen L, Chu S, Doll MA, Li X, Feng W, Siskind L, McClain CJ, and Deng Z (2021). Neutral ceramidase mediates nonalcoholic steatohepatitis by regulating monounsaturated fatty acids and gut IgA(+) B cells. Hepatology 73, 901–919. [PubMed: 33185911]

Habrukowich C, Han DK, Le A, Rezaul K, Pan W, Ghosh M, Li ZG, Dodge-Kafka K, Jiang XJ, Bittman R, et al. (2010). Sphingosine interaction with acidic leucine-rich nuclear phosphoprotein-32a (ANP32A) regulates PP2A activity and cyclooxygenase (COX)-2 expression in human endothelial cells. J. Biol. Chem 285, 26825–26831. [PubMed: 20558741]

Huang SCC, Everts B, Ivanova Y, O'Sullivan D, Nascimento M, Smith AM, Beatty W, Love-Gregory L, Lam WY, O'Neil CM, et al. (2014). Cell-intrinsic lysosomal lipolysis is essential for alternative activation of macrophages. Nat. Immunol 15, 846–855. [PubMed: 25086775]

Kim YG, Kamada N, Shaw MH, Warner N, Chen GY, Franchi L, and Nunez G (2011). The Nod2 sensor promotes intestinal pathogen eradication via the chemokine CCL2-dependent recruitment of inflammatory monocytes. Immunity 34, 769–780. [PubMed: 21565531]

Kim YG, Sakamoto K, Seo SU, Pickard JM, Gillilland MG 3rd, Pudlo NA, Hoostal M, Li X, Wang TD, Feehley T, et al. (2017). Neonatal acquisition of Clostridia species protects against colonization by bacterial pathogens. Science 356, 315–319. [PubMed: 28428425]

Kono M, Dreier JL, Ellis JM, Allende ML, Kalkofen DN, Sanders KM, Bielawski J, Bielawska A, Hannun YA, and Proia RL (2006). Neutral ceramidase encoded by the Asah2 gene is essential for the intestinal degradation of sphingolipids. J. Biol. Chem 281, 7324–7331. [PubMed: 16380386]

Koroleva EP, Halperin S, Gubernatorova EO, Macho-Fernandez E, Spencer CM, and Tumanov AV (2015). Citrobacter rodentium-induced colitis: a robust model to study mucosal immune responses in the gut. J. Immunol. Methods 421, 61–72. [PubMed: 25702536]

Lang J, Bohn P, Bhat H, Jastrow H, Walkenfort B, Cansiz F, Fink J, Bauer M, Olszewski D, Ramos-Nascimento A, et al. (2020). Acid ceramidase of macrophages traps herpes simplex virus in multivesicular bodies and protects from severe disease. Nat. Commun 11, 1338. [PubMed: 32165633]

Langston PK, Nambu A, Jung J, Shibata M, Aksoylar HI, Lei JH, Xu PN, Doan MT, Jiang H, MacArthur MR, et al. (2019). Glycerol phosphate shuttle enzyme GPD2 regulates macrophage inflammatory responses (vol 20, pg 1186, 2019). Nat. Immunol 20, 1555.

Leishman AJ, Naidenko OV, Attinger A, Koning F, Lena CJ, Xiong Y, Chang HC, Reinherz E, Kronenberg M, and Cheroutre H (2001). T cell responses modulated through interaction between CD8 alpha alpha and the nonclassical MHC class I molecule, TL. Science 294, 1936–1939. [PubMed: 11729321]

Liang J, Nagahashi M, Kim EY, Harikumar KB, Yamada A, Huang WC, Hait NC, Allegood JC, Price MM, Avni D, et al. (2013). Sphingosine-1-phosphate links persistent STAT3 activation, chronic intestinal inflammation, and development of colitis-associated cancer. Cancer Cell 23, 107–120. [PubMed: 23273921]

Luheshi NM, Giles JA, Lopez-Castejon G, and Brough D (2012). Sphingosine regulates the NLRP3-inflammasome and IL-1 ss release from macrophages. Eur. J. Immunol 42, 716–725. [PubMed: 22105559]

Maceyka M, and Spiegel S (2014). Sphingolipid metabolites in inflammatory disease. Nature 510, 58–67. [PubMed: 24899305]

Meiners J, Palmieri V, Klopfleisch R, Ebel JF, Japtok L, Schumacher F, Yusuf AM, Becker KA, Zoller J, Hose M, et al. (2019). Intestinal acid sphingomyelinase protects from severe pathogen-driven colitis. Front. Immunol 10, 1386. [PubMed: 31275322]

Moon JS, Hisata S, Park MA, DeNicola GM, Ryter SW, Nakahira K, and Choi AMK (2015). mTORC1-Induced HK1-dependent glycolysis regulates NLRP3 inflammasome activation. Cell Rep. 12, 102–115. [PubMed: 26119735]

Mullineaux-Sanders C, Sanchez-Garrido J, Hopkins EGD, Shenoy AR, Barry R, and Frankel G (2019). Citrobacter rodentium-host-microbiota interactions: immunity, bioenergetics and metabolism. Nat. Rev. Microbiol 17, 701–715. [PubMed: 31541196]

Navabi N, Whitt J, Wu SE, Woo V, Moncivaiz J, Jordan MB, Vallance BA, Way SS, and Alenghat T (2017). Epithelial histone deacetylase 3 instructs intestinal immunity by coordinating local lymphocyte activation. Cell Rep. 19, 1165–1175. [PubMed: 28494866]

Norris GH, Jiang C, Ryan J, Porter CM, and Blesso CN (2016a). Milk sphingomyelin improves lipid metabolism and alters gut microbiota in high fat diet-fed mice. J. Nutr. Biochem 30, 93–101. [PubMed: 27012625]

Norris GH, Jiang C, Ryan J, Porter CM, and Blesso CN (2016b). Milk sphingomyelin improves lipid metabolism and alters gut microbiota in high fat diet-fed mice. J. Nutr. Biochem 30, 93–101. [PubMed: 27012625]

Oaks J, and Ogretmen B (2015). Regulation of PP2A by sphingolipid metabolism and signaling. Front. Oncol 4, 388. [PubMed: 25642418]

Pham TAN, and Lawley TD (2014). Pathogens' exploitation of the intestinal food web. Cell Host Microbe 16, 703–705. [PubMed: 25498340]

Ramanan D, and Cadwell K (2016). Intrinsic defense mechanisms of the intestinal epithelium. Cell Host Microbe 19, 434–441. [PubMed: 27049583]

Rivollier A, He JP, Kole A, Valatas V, and Kelsall BL (2012). Inflammation switches the differentiation program of Ly6C(hi) monocytes from antiinflammatory macrophages to inflammatory dendritic cells in the colon. J. Exp. Med 209, 139–155. [PubMed: 22231304]

Schreiber HA, Loschko J, Karssemeijer RA, Escolano A, Meredith MM, Mucida D, Guermonprez P, and Nussenzweig MC (2013). Intestinal monocytes and macrophages are required for T cell polarization in response to Citrobacter rodentium. J. Exp. Med 210, 2025–2039. [PubMed: 24043764]

Solaymani-Mohammadi S, and Berzofsky JA (2019). Interleukin 21 collaborates with interferon- for the optimal expression of interferon-stimulated genes and enhances protection against enteric microbial infection. PLoS Pathog. 15, e1007614. [PubMed: 30818341]

Stutz A, Kolbe CC, Stahl R, Horvath GL, Franklin BS, van Ray O, Brinkschulte R, Geyer M, Meissner F, and Latz E (2017). NLRP3 inflammasome assembly is regulated by phosphorylation of the pyrin domain. J. Exp. Med 214, 1725–1736. [PubMed: 28465465]

Tannahill GM, Curtis AM, Adamik J, Palsson-McDermott EM, McGettrick AF, Goel G, Frezza C, Bernard NJ, Kelly B, Foley NH, et al. (2013). Succinate is an inflammatory signal that induces IL-1 beta through HIF-1 alpha. Nature 496, 238. [PubMed: 23535595]

Thiemann S, Smit N, Roy U, Lesker TR, Galvez EJC, Helmecke J, Basic M, Bleich A, Goodman AL, Kalinke U, et al. (2017). Enhancement of IFN gamma production by distinct commensals ameliorates salmonella-induced disease. Cell Host Microbe 21, 682. [PubMed: 28618267]

Tschopp J, and Schroder K (2010). NLRP3 inflammasome activation: the convergence of multiple signalling pathways on ROS production? Nat. Rev. Immunol 10, 210–215. [PubMed: 20168318]

Van den Bossche J, O'Neill LA, and Menon D (2017). Macrophage immunometabolism: where are we (going)? Trends Immunol. 38, 395–406. [PubMed: 28396078]

Xie M, Yu Y, Kang R, Zhu S, Yang LC, Zeng L, Sun XF, Yang MH, Billiar TR, Wang HC, et al. (2016). PKM2-dependent glycolysis promotes NLRP3 and AIM2 inflammasome activation. Nat. Commun 7, 13280. [PubMed: 27779186]

Zheng Y, Valdez PA, Danilenko DM, Hu Y, Sa SM, Gong Q, Abbas AR, Modrusan Z, Ghilardi N, de Sauvage FJ, et al. (2008). Interleukin-22 mediates early host defense against attaching and effacing bacterial pathogens. Nat. Med 14, 282–289. [PubMed: 18264109]

Highlights

- Neutral ceramidase (NcDase) controls intestinal immune cell dynamics
- NcDase in intestinal macrophages is necessary for defense against bacterial infection
- Sphingosine drives macrophage glycolysis and enhances macrophage bactericidal activity
- Dietary sphingomyelin can protect against *C. rodentium* infection

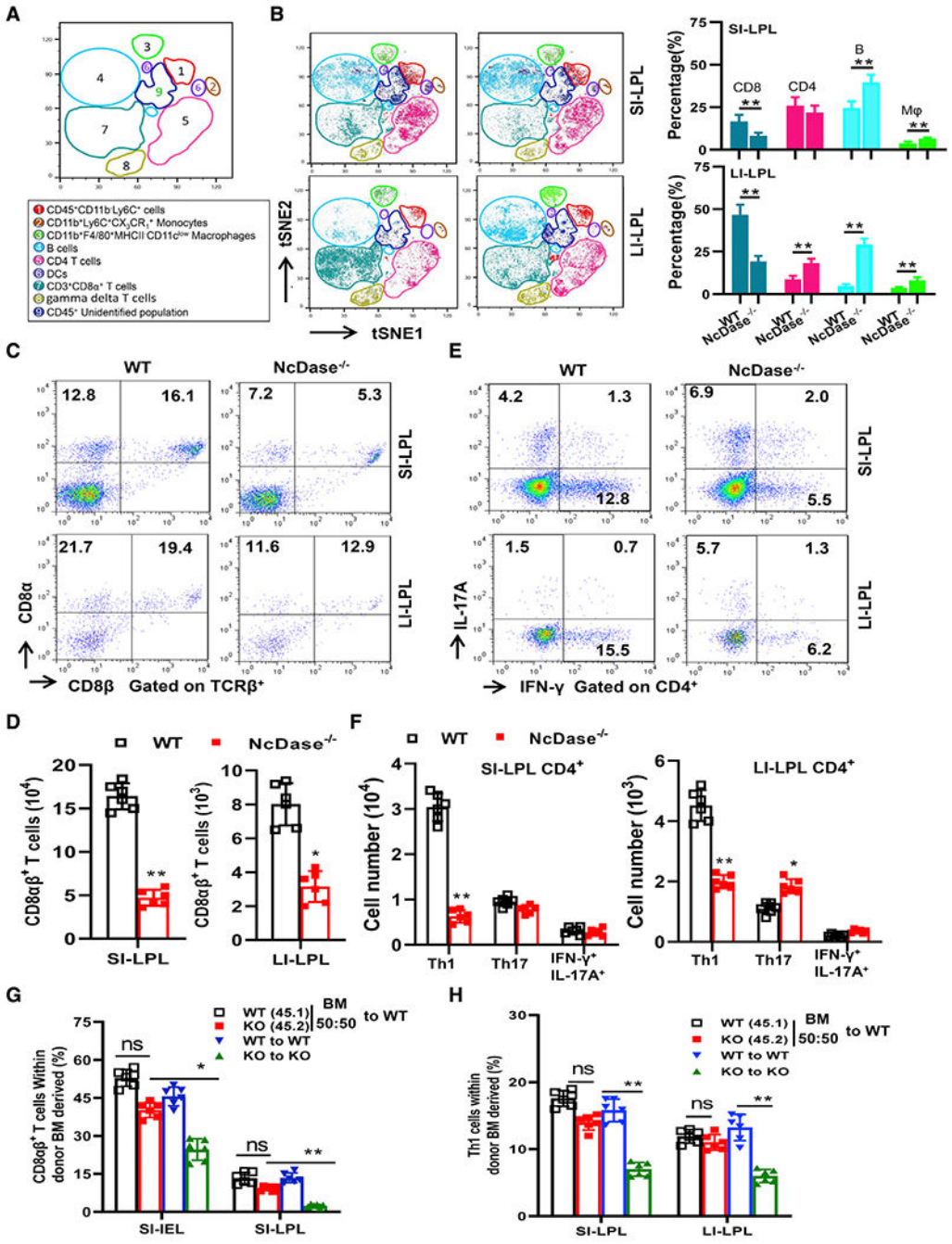

Figure 1. Impact of NcDase deletion on immune cell homeostasis in the lamina propria

(A) Schematic representation of clustering after CyTOF analysis of lamina propria lymphocytes (LPL) from large intestine (LI-LPL) or small intestine (SI-LPL) in naive WT and NcDase$^{-/-}$ mice.

(B) Dot plot representation of t-distributed stochastic neighbor embedding (tSNE) analysis and percentage analysis showing different clusters that enable the distinction of immune populations.

(C) FACS analysis of CD8αβ$^+$ (CD8α$^+$CD8β$^+$) and CD8αα$^+$ (CD8α$^+$CD8β$^-$) T cells in the SI-LPL or LI-LPL.

(D) Quantitative analysis of CD8αβ$^+$ T cells in SI-LPL or LI-LPL in WT and NcDase$^{-/-}$ mice.

(E and F) Intracellular staining (E) and quantitative analysis (F) of IL-17A and IFN-γ in CD4$^+$ T cells in the LI-LPL or SI-LPL.

(G and H) Single or mixed BM were transferred to indicated receipt mice. FACS analysis of CD8αβ$^+$ and CD8αα$^+$ T cells (G) and Th1 cells (H) in the SI-LPL, SI-IEL, or LI-LPL. Data are from (A, B) wo, (C-F) two or three, or (G and H) two independent experiments. Each dot represents one mouse. Here and thereafter, error bars represent mean ± SEM. *p <0.05, **p <0.01. ns, not significant from nonparametric t tests unless otherwise specified. See also Figures S1 and S2.

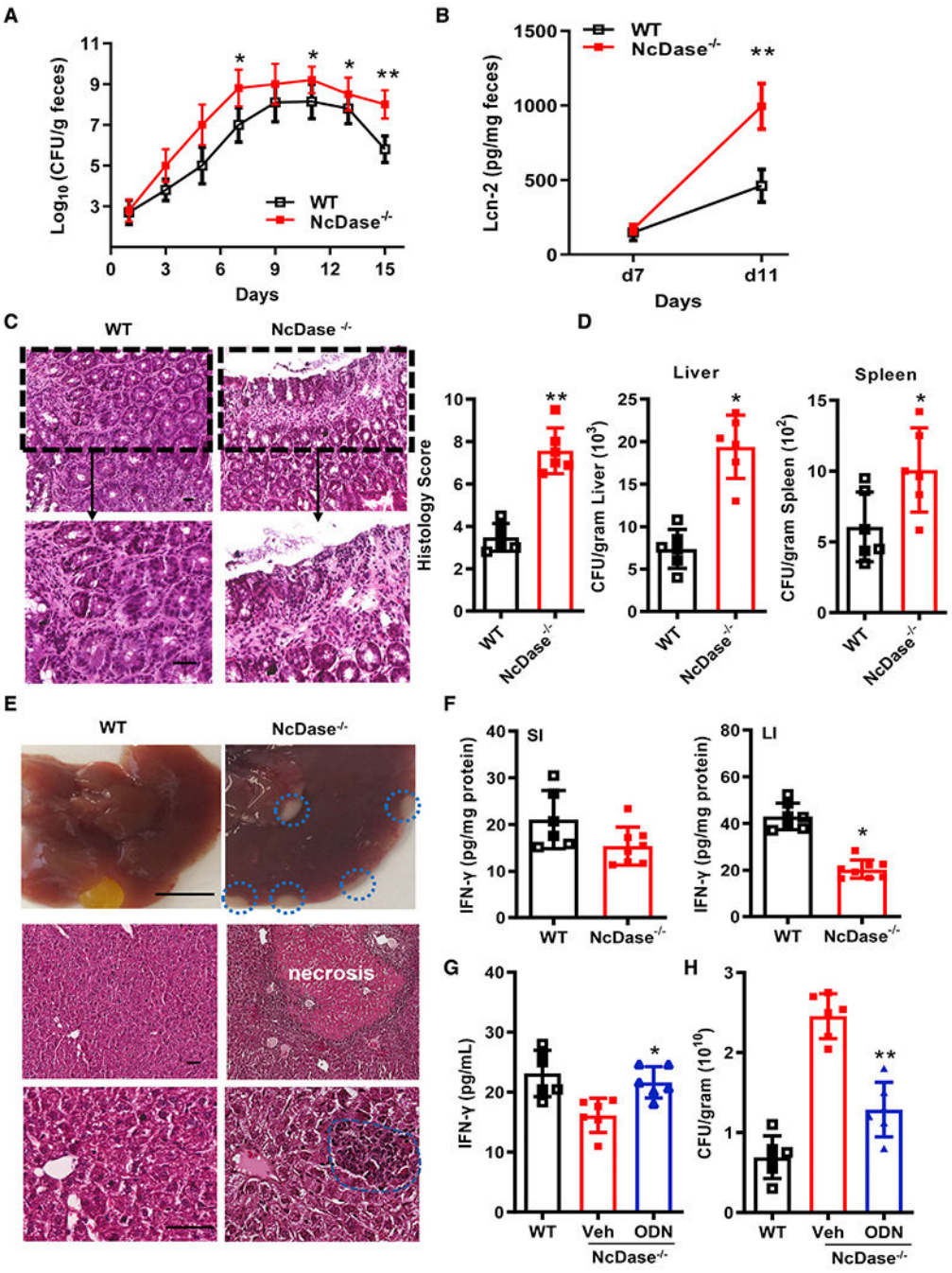

Figure 2. NcDase mutant mice are susceptible to *C. rodentium* infection

WT littermates and NcDase$^{-/-}$ mice were orally infected with 2 × 10^9 CFU *C. rodentium.*

(A) Bacteria recovered from stools over time after mice inoculated with *C. rodentium.*

(B) Lipocalin-2 (Lcn-2) levels in the feces of mice infected with *C. rodentium.*

(A and B) Pooled results of two experiments, total 10 mice per group, mean ± SEM, *p < .05, **p <0.01.

(C) Representative H&E staining of three experiments and histologic scores from six mice per group for colonic pathology at day 12 post infection. Scale bar, 50 μm.

(D) Bacteria recovered from liver and spleen. Representative results of two experiments. n = 6, mean ± SEM, *p <0.05.

(E) Gross areas of necrosis (blue circle, top, Scale bar, 5 mm.) and H&E staining of liver sections (middle and bottom, scale bar, 50 μm). Representative results of two experiments, n = 6 per group.

(F) IFN-γ in large intestine (LI) and small intestine (SI) measured by ELISA 6 days post infection. n = 6, mean ± SEM, *p <0.05.

(G) IFN-γ in colonic tissue 6 days post infection following treatment with PBS or Th1-inducing ODN-BW006.

(H) *C. rodentium* CFUs in stool of mice treated as in (G).

(F–H) Representative results of two experiments, mean ± SEM, n = 6,*p <0.05, **p <0.01. Each dot represents one mouse. Error bars represent mean ± SEM. See also Figure S3.

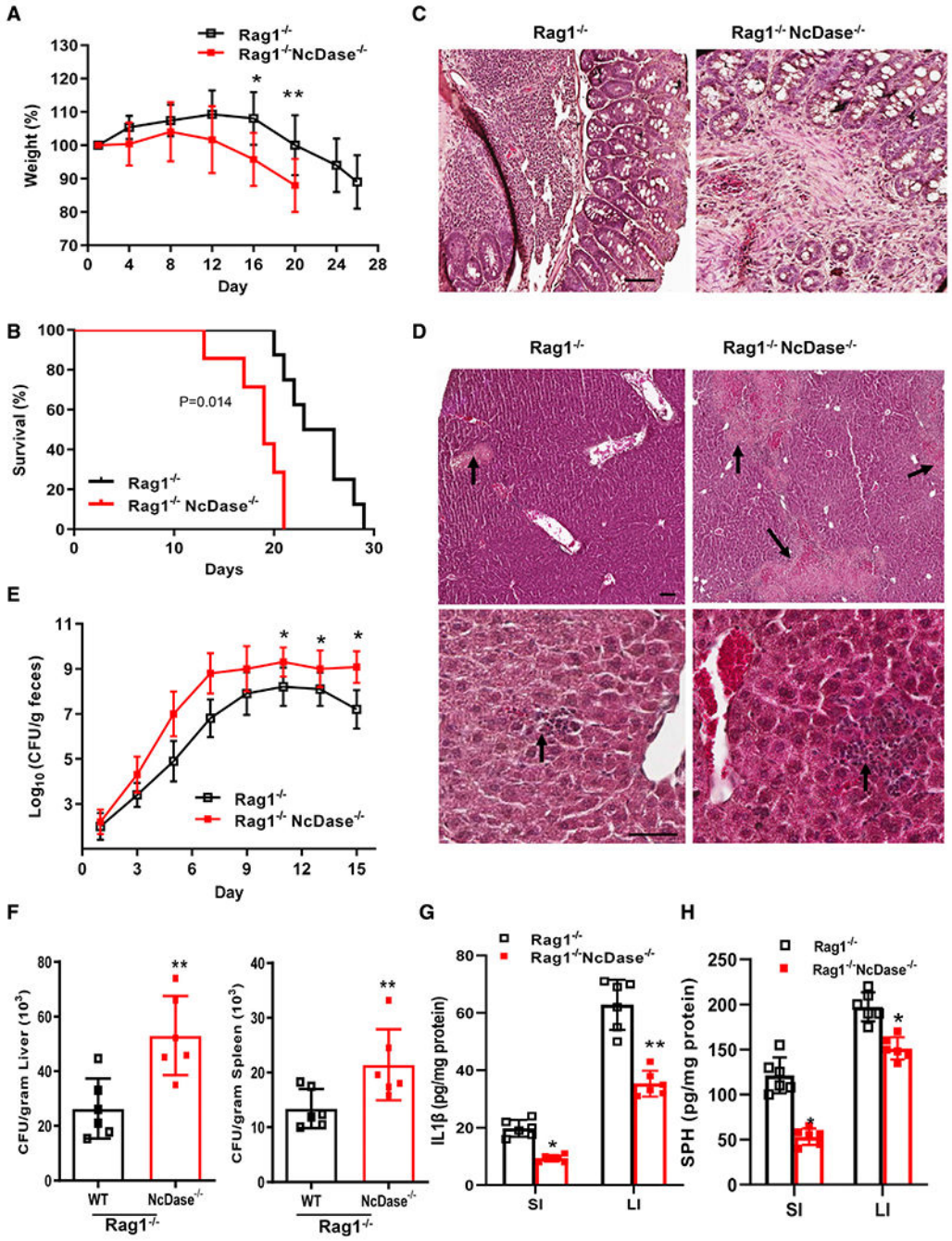

Figure 3. NcDase is crucial for innate immune responses against *C. rodentium* infection

$Rag1^{-/-}$ $NcDase^{-/-}$ mice and $Rag1^{-/-}$ littermates were orally inoculated with 2×10^9 CFU *C. rodentium.*

(A and B) Body weight change (A) and survival rates (B) of the mice at the indicated time points. n = 8.

(C and D) H&E staining of colon (C) and liver sections (D) in infected mice. Arrow shows necrosis and hepatic embolic microabscess. Scale bar, 50 μm. (E and F) Bacteria recovered from stools, liver, and spleen.

(G) IL-1β in the ileum and colonic tissue 6 days post infection, n = 6.
(H) Sphingosine in the ileum and colonic tissue 6 days post infection, n = 6. The log rank test was used to compare survival differences (B), and continuous variables were analyzed by nonparametric t tests (A, E, F, G, H). Data are from two independent experiments. Each dot represents one mouse, n = 6. Error bars represent mean ± SEM. *p <0.05, **p <0.01. See also Figure S5.

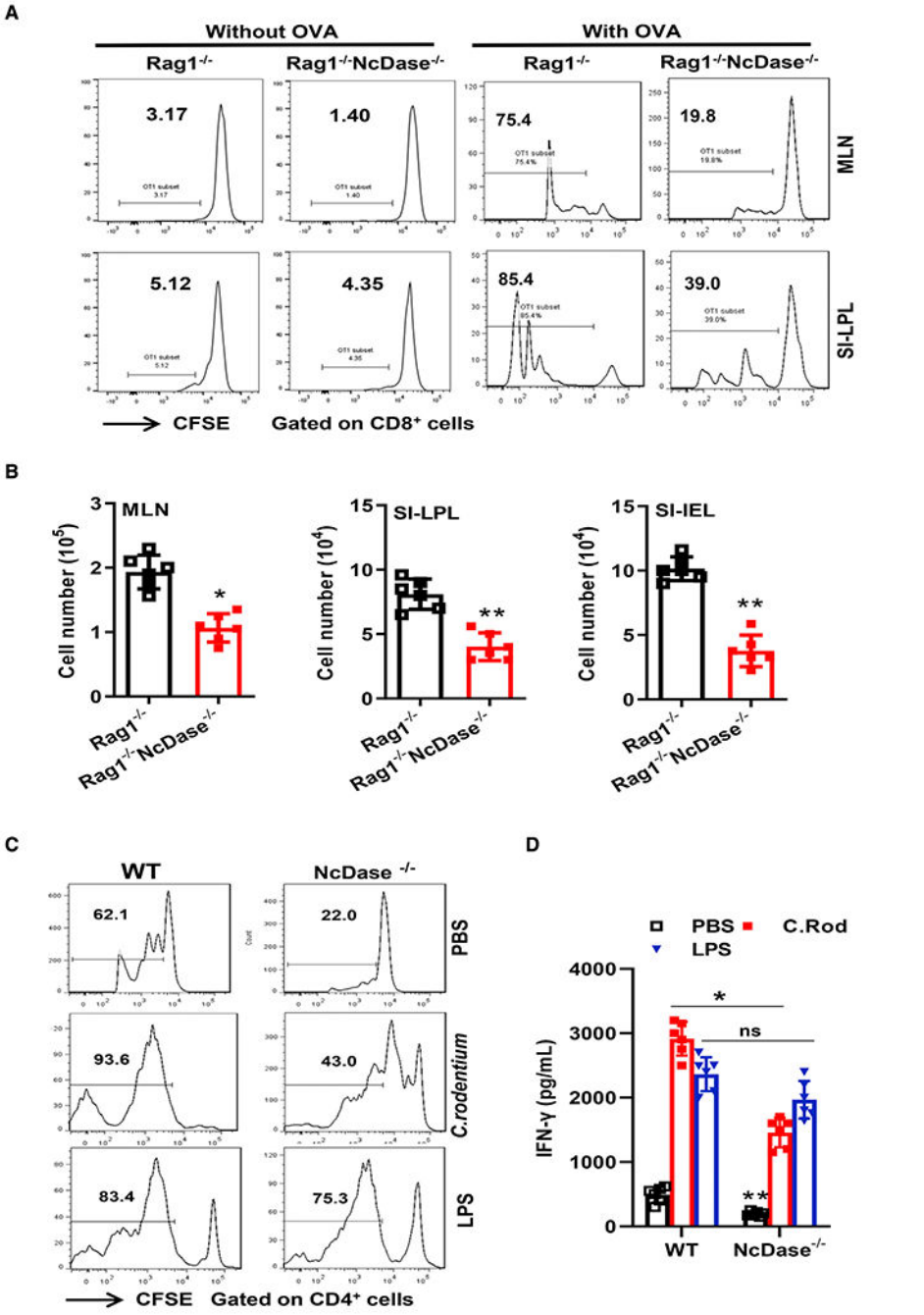

Figure 4. Macrophage NcDase is required for initiating adaptive immune responses

(A and B) CFSE-labeled OT-I cells were transferred into Rag1$^{-/-}$ NcDase$^{-/-}$ or Rag1$^{-/-}$ mice.

(A) Division history of OT-I cells in the MLN and SI-LPL by flow cytometry plots.

(B) Total number of OT-I cells in the MLN, SI-LPL, and SI-IEL of recipient mice 2 days (MLN) and 3 days (SI) after oral gavage with OVA.

(C) CFSE-labeled OT-II cells were co-cultured with PBS-, *C. rodentium*-, and LPS-derived BMDMs in the presence of OVA. FACS analysis of division history of OT-II cells.

(D) ELISA analysis of IFN-γ in the supernatant from (C) Data are representative results (A, C) or combined results (B, D) from three independent experiments, total n = 6 per groups. Error bars represent mean ± SEM. *p <0.05, **p <0.01.

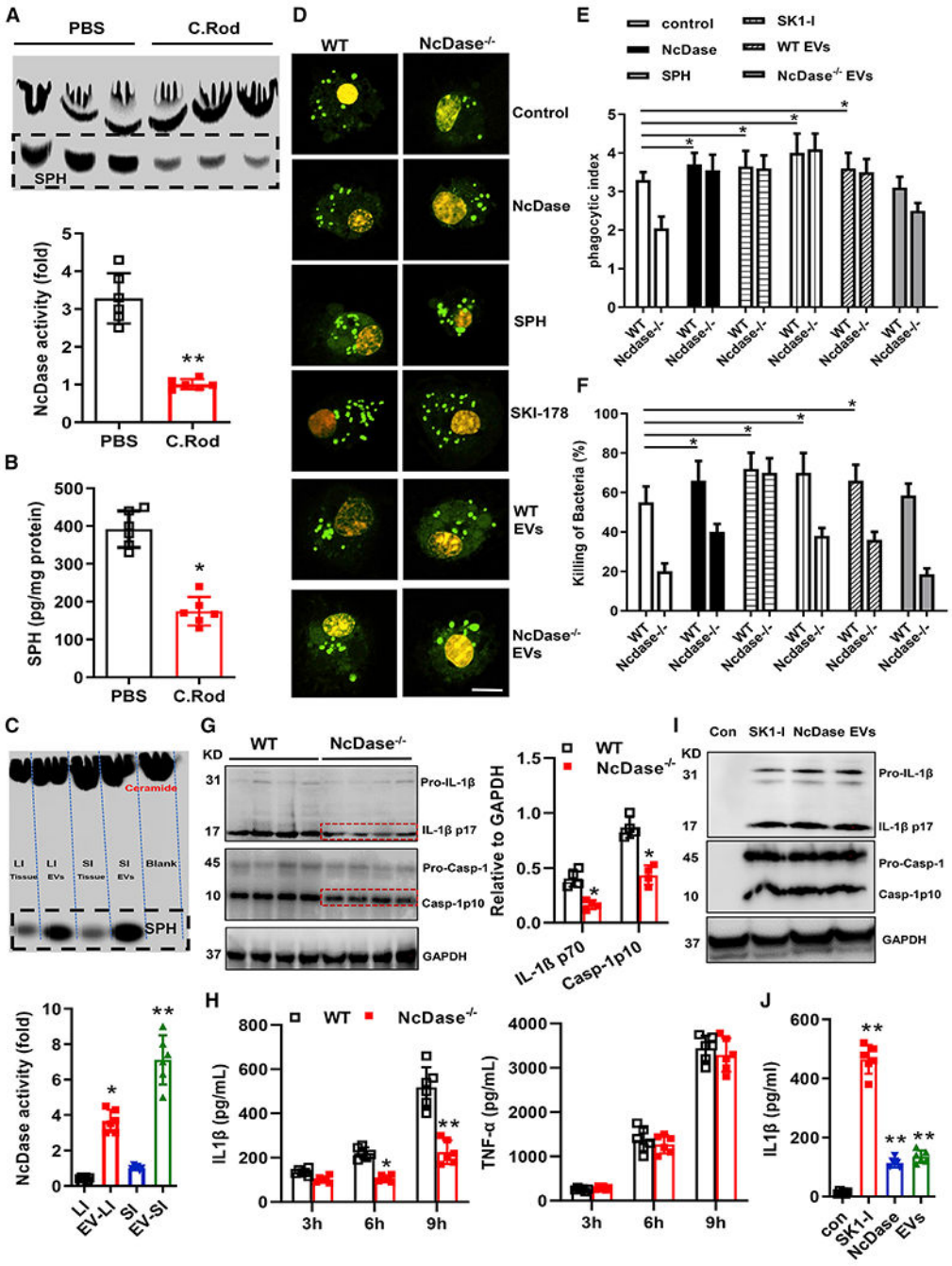

Figure 5. NcDase modulates IL-1β release and the activation of NLRP3 inflammasome in macrophages

(A–C) C56BL/6J mice were orally infected with *C. rodentium*, and tissues were collected and analyzed 10 days post infection.

(A) NcDase activity in the colon in naive and infected mice. Colonic protein was incubated with NBD C12-ceramide at 37°C for 3 h, and lipids were separated by thin-layer chromatography (TLC) plate and detected using a luminescent image analyzer. Released sphingosine from ceramide indicates the activity of NcDase.

(B) Level of sphingosine in the colon.

(C) NcDase activity in the tissues or EVs from LI and SI in naive mice. Released sphingosine indicates the activity of NcDase, which is shown as a graph. Data are from (A-C) 2 independent experiments. n = 3 per experiment. Each dot represents one mouse. Error bars represent mean ± SEM. *p <0.05, **p <0.01.

(D-F) Bone marrow-derived macrophages (BMDMs) from WT and NcDase$^{-/-}$ mice were treated with CFSE-labeled (D and E) or unlabeled 10^7 CFU/mL *C. rodentium* (F) in the presence of control vehicle, recombinant NcDase protein, SPH, SphK1 inhibitor SKI-178 (SK1-I), EVs from WT mice, or EVs from NcDase$^{-/-}$ mice.

(D and E) Bacterial phagocytosis by macrophages. Scale bar, 10 μm.

(F) Bacterial killing by macrophages. Data are representative (D) or pooled results from (E and F) two independent experiments. Total n = 8–10 per group. Error bars represent mean ± SEM. *p <0.05.

(G) Immunoblotting and qualification for procaspase-1 and activated caspase-1 (p10), pro-IL-1β, and cleaved IL-1β (p17) in supernatants and GAPDH in cell lysates from Lipopolysaccharides (LPS)-primed BMDMs.

(H) ELISA for IL-1β and TNF-α in supernatants of LPS-primed BMDMs.

(I) Immunoblotting for procaspase-1 and activated caspase-1 (p10), pro-IL-1β, and cleaved IL-1β (p17) in supernatants of LPS-primed BMDMs stimulated with vehicle, SK1-178 (SK1-I), NcDase protein, or NcDase^{+} EVs.

(J) ELISA for IL-1β in supernatants from (I). Data are representative (G and I) or pooled results from (H and J) two independent experiments, each dot represents one mouse, n = 6. Error bars represent mean ± SEM. *p <0.05, **p <0.01. See also Figure S6.

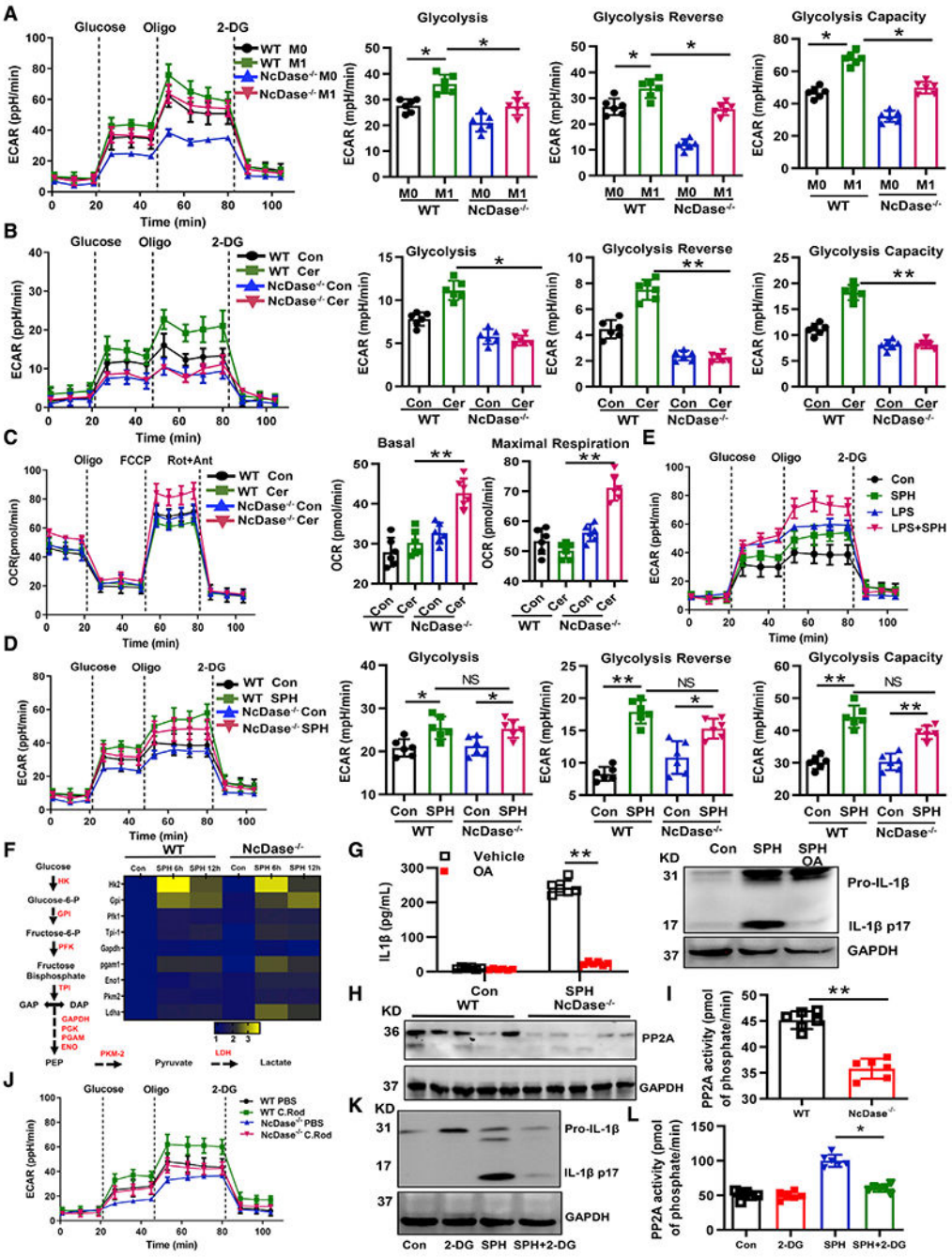

Figure 6. Sphingosine promotes glycolysis in macrophages

(A) ECAR of glycolysis, glycolytic reserve, and capacity in WT and NcDase$^{-/-}$ macrophages treated with PBS (M0) or LPS + IFN-γ (M1) for 17 h and given sequential treatment with oligomycin and 2-deoxyglucose (2-DG).

(B) ECAR of glycolysis, glycolytic reserve, and capacity in WT and NcDase$^{-/-}$ macrophages treated with DMSO (Con) or 20 μM ceramide (Cer) for 17 h and given sequential treatment with oligomycin and 2-DG.

(C) OCR, basal respiratory capacity, and maximal respiratory capacity in WT and NcDase$^{-/-}$ macrophages treated with DMSO (Con) or 20 μM ceramide (Cer) for 17 h and given sequential treatment with oligomycin, fluoro-carbonyl cyanide phenylhydrazone (FCCP), and rotenone plus antimycin (Rot + ant).
(D) ECAR of glycolysis, glycolytic reserve, and capacity in WT and NcDase$^{-/-}$ macrophages treated with DMSO (Con) or 25 μM sphingosine (SPH) for 3 h and given sequential treatment with oligomycin and 2-DG.
(E) ECAR of glycolysis in LPS-primed or unprimed BMDMs treated with DMSO (Con) or 25 μM sphingosine (SPH) for 3 h and given sequential treatment with oligomycin and 2-DG. (A–E) Mean ± SEM; *p <0.05 and **p <0.01 (nonparametric t tests). Data are representative or pooled results from three independent experiments, total n = 6 per group, each dot represents one mouse.
(F) The glycolytic pathway (left) with the metabolic genes measured highlighted in red. RNA was isolated from macrophages and collected at the indicated times after sphingosine treatment and used for qPCR analyses of metabolic genes in the glycolytic pathway (right). mRNA levels in resting WT macrophages were set to 1. The heatmap represents the fold of the relative mRNA expression level (see color scale).
(G) ELISA and immunoblotting for IL-1β in supernatants of LPS-primed and vehicle-or SPH-stimulated BMDMs in the presence of vehicle or OA. (F and G) Data are pooled results from three independent experiments, total n = 6 per group, mean ± SEM; **p <0.01.
(H) Representative immunoblotting for PP2A in the colonic tissue from *C. rodentium*-infected mice.
(I) The activity of PP2A in the colonic tissue from *C. rodentium*-infected mice.
(J) ECAR of glycolysis, glycolytic reserve, and capacity in WT and NcDase$^{-/-}$ macrophages isolated from colon after infection. Data are from (H and I) two or (J) three independent experiments. Total n = 6. Error bars represent mean ± SEM. **p <0.01.
(K) Immunoblotting for IL-1β, procaspase-1, and activated caspase-1 (p10) in supernatants of LPS-primed and vehicle-or SPH-stimulated BMDMs in the presence of vehicle or 2-DG.
(L) The activity of PP2A in LPS-primed macrophages treated with vehicle-or SPH in the presence of vehicle or 2-DG. Data are representative (K) or pooled results (L) from three independent experiments, each dot represents one mouse, total n = 6 per group. Error bars represent mean ± SEM. *p <0.05.

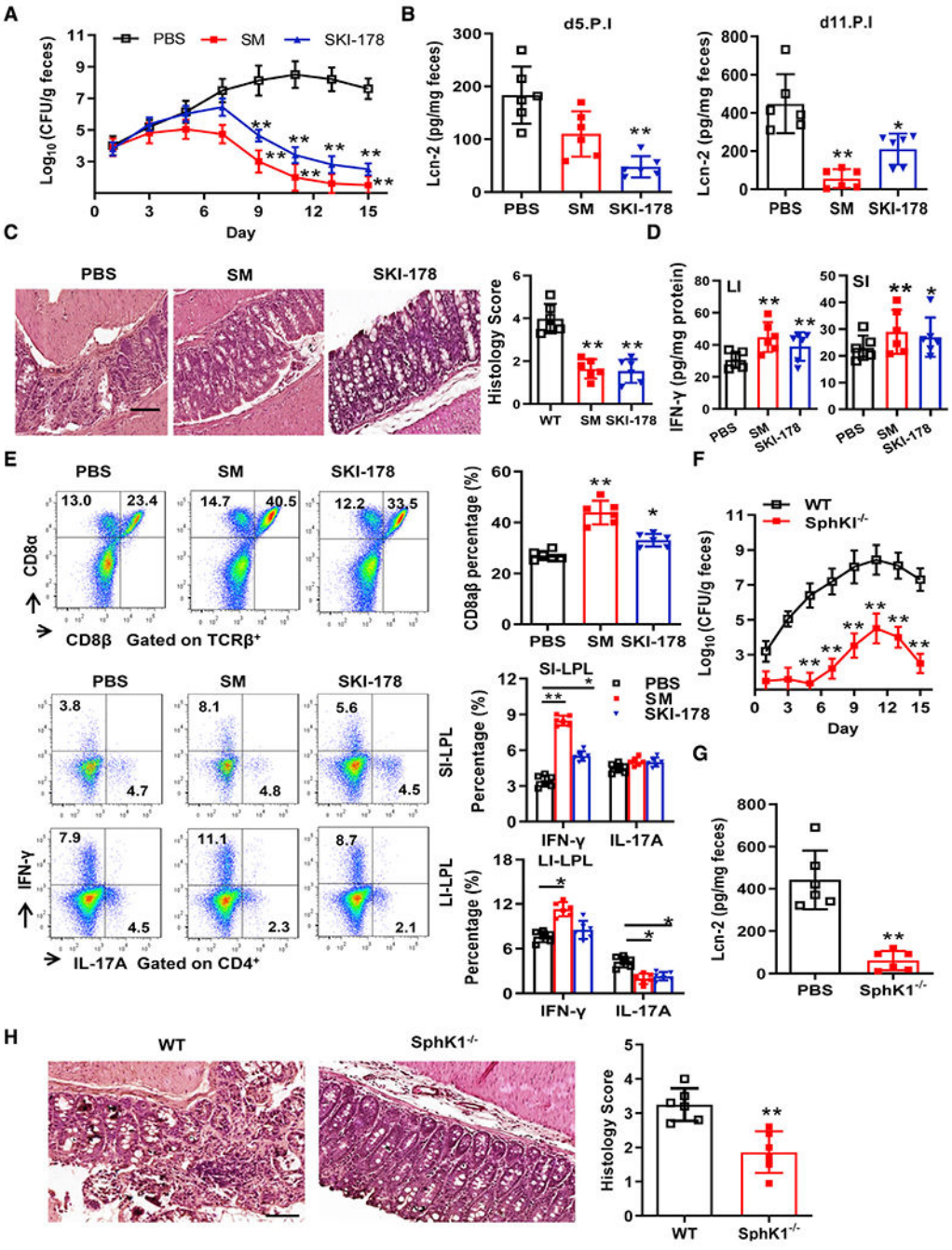

Figure 7. Increase of sphingosine prevents pathogen colonization in the gut

(A–G) C57BL/6J mice were fed 12.5 mg of extracted sphingomyelin per day at 1 week before and after infection or treated with SKI-178 (10 mg/kg, intraperitoneally [i.p.]) every other day after 2×10^9 CFU *C. rodentium* infection.

(A) *C. rodentium* loads in feces.

(B) The level of fecal lipocalin-2.

(C) H&E staining of colon. Scale bar, 50 μm.

(D) ELISA analysis of IFN-γ in the intestine.

(E) FACS staining of CD8αβ$^+$ T cells or IL-17A and IFN-γ in CD4$^+$ T cells in SI- and LI-LPL. Data show representative (C) or combined (A and B, D and E) results from two independent experiments; each dot represents one mouse. Total n = 6, *p <0.05, **p <0.01.
(F–H) WT and Sphk1$^{-/-}$ mice were orally infected with *C. rodentium.*
(F) *C. rodentium* loads in feces.
(G) The level of fecal lipocalin-2.
(H) H&E staining of colon. Scale bar, 50 μm. Data show representative (H) or combined (F and G) results from at least three independent experiments, each dot represents one mouse. Mean ± SEM; n = 6–7, **p <0.01. See also Figure S7.

KEY RESOURCES TABLE

REAGENT or RESOURCE	SOURCE	IDENTIFIER
Antibodies		
EpCAM-APC	Thermo Fisher Scientific	Cat# 17-5791-82; RRID: AB_2716944
anti-IFN-γ-PE-Cy7	Thermo Fisher Scientific	Cat# 25-7311-82; RRID: AB_469680
anti-IFN-γ-PE	Thermo Fisher Scientific	Cat# 12-7311-82; RRID: AB_466193
anti-IL-10-APC	Thermo Fisher Scientific	Cat# 17-7101-82; RRID: AB_469502
anti-IL-10-PE	Thermo Fisher Scientific	Cat# 12-7101-41; RRID: AB_10669561
anti-IL-17A-APC	Thermo Fisher Scientific	Cat# 17-7177-81; RRID: AB_763580
anti-IL-17A-PerCP	Thermo Fisher Scientific	Cat# 45-7177-82; RRID: AB_925753
anti-IL-17A-FITC	Thermo Fisher Scientific	Cat# 11-7177-81; RRID: AB_763581
anti-Foxp3-FITC	Thermo Fisher Scientific	Cat# MA1-41628; RRID: AB_1074471
anti-Foxp3-PE	Thermo Fisher Scientific	Cat# 12-4774-42; RRID: AB_10670338
anti-CD11b-PE	Thermo Fisher Scientific	Cat# 12-0112-82; RRID: AB_2734869
anti-CD11b-FITC	Thermo Fisher Scientific	Cat# 11-0112-82; RRID: AB_464935
anti-CD11b-APC	Thermo Fisher Scientific	Cat# 17-0112-82; RRID: AB_469343
Gr-1-PE	Thermo Fisher Scientific	Cat# 12-5931-83; RRID: AB_466046
anti-Gr1-APC	Thermo Fisher Scientific	Cat# 17-5931-82; RRID: AB_469476
anti-ly6G-PE	Thermo Fisher Scientific	Cat# 12-9668-82; RRID: AB_2572720
anti-ly6G-FITC	Thermo Fisher Scientific	Cat# 11-9668-82; RRID: AB_2572532
anti-CD45.2-APC,	Thermo Fisher Scientific	Cat# 17-0454-82; RRID: AB_469400
anti-CD45.1-PerCP	Thermo Fisher Scientific	Cat# 45-0453-82; RRID: AB_1107003
anti-CD45-FITC	Thermo Fisher Scientific	Cat# 11-0451-82; RRID: AB_465050
anti-CD45-Percp	Thermo Fisher Scientific	Cat# 45-0451-82; RRID: AB_1107002
anti-CD45-Pacific Blue	Thermo Fisher Scientific	Cat# MCD4528; RRID: AB_10373710
anti-Sca1-PE	Thermo Fisher Scientific	Cat# 12-5981-82; RRID: AB_466086
anti-S1PR1-PE	R&D System	Cat# *FAB7089P*; RRID: AB_10994187
Anti-CD8α-FITC	Thermo Fisher Scientific	Cat# 11-0081-82; RRID: AB_464915
Anti-CD8β-APC	Thermo Fisher Scientific	Cat# 17-0083-81; RRID: AB_657760
Anti-Granzyme B-FITC	Thermo Fisher Scientific	Cat# 11-8898-82; RRID: AB_10733414
Anti-TCRβ-PE	Thermo Fisher Scientific	Cat# 12-5961-82; RRID: AB_466066
Anti-TCRγδ-APC	Thermo Fisher Scientific	Cat# 17-5711-82; RRID: AB_842756
Anti-CD103-PE	Thermo Fisher Scientific	Cat# 12-1031-82; RRID: AB_465799
Anti-F4/80-PerCP	Thermo Fisher Scientific	Cat# 45-4801-82; RRID: AB_914345
Anti-F4/80-PE	Thermo Fisher Scientific	Cat# 12-4801-82; RRID: AB_465923
Anti-F4/80-APC	Thermo Fisher Scientific	Cat# MF48005; RRID: AB_10375306
Anti-IL-1β	Abcam	Cat# ab9722; RRID: AB_308765
Anti-PP2A	Sigma	Cat# 05-421; RRID: AB_10784862
Anti-Caspase 1	Thermo Fisher Scientific	Cat# 14-9832-82, RRID: AB_2016691

REAGENT or RESOURCE	SOURCE	IDENTIFIER
Anti-GAPDH	Cell signaling	Cat# 5174; RRID: AB_10622025
Goat anti-Rabbit Alexa Fluor 594	Thermo Fisher Scientific	Cat# A32740; RRID: AB_2762824
Goat anti-Rabbit Alexa Fluor 680	Thermo Fisher Scientific	Cat# A32734; RRID: AB_2633283
Goat anti-Mouse Alexa Fluor 488	Thermo Fisher Scientific	Cat# A32723; RRID: AB_2633275
Ly6G (141 Pr)	Fluidigm	Cat# 3141008B; RRID: AB_2814678
CD11c (142 Nd)	Fluidigm	Cat# 3142003B; RRID: AB_2814737
CD8a (168Er)	Fluidigm	Cat# 3168003B; RRID: AB_2811241
CD11b (172Yb)	Fluidigm	Cat# 3172012B; RRID: AB_2661809
CD19 (149 Sm)	Fluidigm	Cat# 3149002B; RRID: AB_2814679
CD25 (151 Eu)	Fluidigm	Cat# 3151007B; RRID: AB_2827880
F4/80 (146 Nd)	Fluidigm	Cat# 3146008B; RRID: AB_2895117
CD36 (147 Sm)	Fluidigm	Cat# 3147018B;RRID:N/A
CD3e (152 Sm)	Fluidigm	Cat# 3152004B; RRID: AB_2687836
CD274 (153Eu)	Fluidigm	Cat# 3153016B; RRID: AB_2687837
CD62L (160 Gd)	Fluidigm	Cat# 3160008B; RRID: AB_2687840
CD73 (154 Sm)	Fluidigm	Cat# 3154019B; RRID: AB_2813854
Ly6c (150Nd)	Fluidigm	Cat# 3150010B; RRID: AB_2895118
CX3CR1 (164 Dy)	Fluidigm	Cat# 3164023B; RRID: AB_2832247
CD103 (163 Dy)	This study	N/A
CD206 (169 Tm)	Fluidigm	Cat# 3169021B; RRID: AB_2832249
NK1.1 (170 Er)	Fluidigm	Cat# 3170002B; RRID: AB_2885023
CD44 (162Dy)	Fluidigm	Cat# 3162030B; RRID: AB_2814898
CD4 (145Nd)	Fluidigm	Cat# 3145002B; RRID: AB_2687832
MHCII (209Bi)	Fluidigm	Cat# 3209006B; RRID: AB_2885025
CD45 (89Y)	Fluidigm	Cat# 3089005B; RRID: AB_2651152
B220 (176 Yb)	Fluidigm	Cat# 3176002B; RRID: AB_2895123
Bacterial and virus strains		
Citrobacter rodentium DBS100	ATCC	Cat# 51459
Salmonella typhimurium CDC 6516–60	ATCC	Cat# 14028
Chemicals, peptides, and recombinant proteins		
Clodronate liposomes	Encapsula NanoSciences	Cat# CLD-8914
Albumin from chicken egg white	Sigma	A5503-5G
Albumin from chicken egg white	Sigma	A2512-1G
Oleic acid	Sigma	O1008
Sphingomyelin	Avanti Polar Lipids	Cat# 860063
Ceramide	Sigma	22244–25MG
Collagenase type 4	Worthington	Cat# LS004189
CellTrace CFSE	Thermo Fisher	Cat# C34554
ODN-BW006	Invivogen	Cat# tlrl-bw006

REAGENT or RESOURCE	SOURCE	IDENTIFIER
LB Broth (Miller)	Sigma	Cat# L3522-250G
D-erythro-Sphingosine	EMD Millipore	Cat# 567726-10MG
SKI-178	Sigma	567732-10MG
Recombinant Mouse ASAH2 Protein	R&D System	Cat# 3558-AH
Hepes	Sigma	Cat# 83264-100ML-F
Percoll	Sigma	Cat# P4937-500ML
Brefeldin A	Sigma	Cat# B7651-5MG
lonomycin	Sigma	Cat# I9657-5MG
PMA	Sigma	Cat#
A740003	Sigma	Cat# 5.083170001
SuperScript™ IV First-Strand Synthesis System	Invitrogen	Cat# 18091050
Ethidium bromide	Sigma	Cat# E7637-5G
Ampicillin	Sigma	Cat# A9393
ECL Western Blotting Substrate	Thermo Fisher Scientific	Cat# 32209
Gill™ Hematoxylin	Thermo Fisher Scientific	Cat# 6765007
Shandon™ Eosin-Y	Thermo Fisher Scientific	Cat# 6766007
Oligomycin	Sigma	Cat# O4876-5G
2-deoxyglucose (2-DG)	Sigma	Cat# D6134-5G
Antimycin A	Sigma	Cat# A8674-25MG
Rotenone	Sigma	Cat# R8875-1G
Fluoro-carbonyl cyanide phenylhydrazone (FCCP)	Sigma	Cat# C2920-10MG
Complete™ Protease Inhibitor Cocktail	Sigma	Cat# 11697498001
NBD C_{12}-ceramide	Cayman Chemical	Cat# 10007958
TLC Silica gel 60	silica gel, Sigma	Cat# HX02024426
Phosphatase Inhibitor Cocktail	Sigma	Cat# P2850
Critical commercial assays		
RNeasy Mini Kit	Qiagen	Cat# 74104
Nunc™ Lab-Tek™ II Chamber Slide™ System	Thermo Fisher	Cat# 154453
IL-1β ELISA kit	Thermo Fisher	Cat# EM2IL1B
TNF-α ELISA kit	Thermo Fisher	Cat# BMS607-3TWO
IL-22 ELISA kit	Thermo Fisher	Cat# 88-7422-88
Lipocalin-2/NGAL ELISA kit	R&D System	Cat# DY-1857-05
IFN-γ ELISA kit	Thermo Fisher	Cat# 88-7314-88
PowerUP™ SYBR™ Green Master Mix	Qiagen	Cat# 204143
Sphingosine ELISA kit	AVIVA SYSTEM BIOLOGY	Cat# OKEH02615
XF96 Sensor Cartridge	Agilent	Cat# W36221
XF96 cell culture plate	Agilent	Cat# 08121
PP2A Immunoprecipitation Phosphatase Assay Kit	Sigma	Cat# 17-313

REAGENT or RESOURCE	SOURCE	IDENTIFIER
Experimental models: Organisms/strains		
C57BL/6	Jackson Laboratory Stock	Cat# 000664
C57BL/6 (CD45.1)	Jackson Laboratory Stock	Cat# 002014
Rag1$^{-/-}$	Jackson Laboratory Stock	Cat# 002216
NcDase$^{-/-}$	Dr. Yusuf A. Hannun (Stony Brook University)	Kono et al. (2006)
C57BL/6-Tg(TcraTcrb)1100Mjb/J (OT-I)	Jackson Laboratory Stock	Cat# 003831
B6.Cg-Tg(TcraTcrb)425Cbn/J (OT-II)	Jackson Laboratory Stock	Cat# 004194
Oligonucleotides		
See Table S1 for oligonucleotide information	This paper	N/A
Software and algorithms		
Prism (GraphPad Software)	GraphPad	https://www.graphpad.com
FlowJo V 10.8	BD Biosciences	https://www.flowjo.com/
R	N/A	https://www.r-project.org/